Role of surface and sub-surface soil moisture for vegetation functioning

Master's Thesis

in the Department of Civil, Geo and Environmental Engineering

School of Engineering and Design

Technical University of Munich.

Supervised by: **Anne Hoek Van Dijke**

Hydrosphere-Biosphere-Climate-Interactions Group (HBCI),

Max Planck Institute for Biogeochemistry (MPI-BGC)

René Orth

Hydrosphere-Biosphere-Climate-Interactions Group (HBCI),

Max Planck Institute for Biogeochemistry (MPI-BGC)

Timo Schaffhauser

Chair of Hydrology and River Basin Management, TUM

Submitted by: **Prajwal Khanal**

037466743

Submitted in: 29.10.2022

Declaration of Authorship

I hereby declare that this submitted thesis is my original work. All direct or indirect sources, used in this study, are acknowledged as references.

Munich, 29.10.2022, Prajwal Khanal

Acknowledgement

Abstract

Soil water availability is a critical requirement for vegetation growth in a water-limited regime. Since rooting depth differs along vegetation types and climatic regimes, the soil moisture at varying depths might be important for the study of plant functioning. However, the influence of vertical variability of soil moisture on vegetation is not well understood. Here, we analyze the role of surface and deep soil moisture on vegetation photosynthesis during the growing season months and the dry months across varying vegetation types. For this, we correlate vegetation photosynthesis, represented by the sun-induced fluorescence and surface and deep soil moisture. We find that vegetation photosynthesis is stronger correlated with surface soil moisture compared to deep soil moisture. Within vegetation types, grasses, shrubs, and savannas are strongly correlated with surface soil moisture compared to the forest of all types. Furthermore, in dry months, photosynthesis in vegetation becomes more sensitive to the surface and sub-surface soil moisture variations compared to growing season months for all vegetation types. This study highlights the potential to study the role of surface and sub-surface soil moisture in vegetation functioning using a truly observational datasets on a global scale.

Contents

List of Figures

List of Tables

1 Introduction

Vegetation regulates the biogeophysical and biogeochemical processes between the land surface and the atmosphere (Bonan, 2015). The biogeophysical process links the biosphere with the atmosphere through the transfer of heat, moisture, and momentum, while the biogeochemical process circulates carbon, nitrogen, and methane between these spheres. Vegetation also controls numerous other processes and feedbacks in the land-atmosphere continuum, like the direct regulation of terrestrial transpiration (Zeng et al., 2018) and indirect regulation of the water cycle through its impact on precipitation and runoff (Hoek van Dijke et al., 2022). Vegetation further provides vital ecosystem services such as food production and is crucial for offsetting anthropogenic carbon dioxide emissions to mitigate climate change as the terrestrial ecosystem absorbs, on average, 30 percent of anthropogenic carbon emissions (Keenan and Williams, 2018).

Vegetation growth depends, among others, upon water, energy, and nutrient availability. In an energy-limited regime, radiation and temperature control vegetation functioning, as these regions typically have ample soil moisture supply. In contrast, soil moisture becomes critical for vegetation growth in a water-limited regime. On leaf scale, plants open stomata to absorb carbon dioxide during photosynthesis and, in the process, lose water through transpiration. However, in water-limited conditions, plants reduce stomata opening to prevent water loss, thereby lowering photosynthesis. Hence, any fluctuations in soil moisture likely explain variation in photosynthesis in water-limited conditions. Climate change has further increased the global extent of water limitation on vegetation (Denissen et al., 2022) and enhanced vegetation sensitivity to soil moisture (Li et al., 2022) . Hence, it becomes imperative to understand how plants' functioning depends upon soil moisture and how vegetation copes with drought to comprehend the future of global water, energy and carbon cycles.

Plants take up water from varying soil depths depending on their rooting location and soil moisture availability. The uptake depth varies spatially across climates and vegetation types and temporally between seasons. Vegetation in arid regions is more sensitive to surface soil moisture fluctuations than vegetation in humid areas (Xie et al., 2019). Similarly, grasses, generally having shorter roots than trees and shrubs, are more dependent upon surface moisture than deeper moisture (Schenk and Jackson, 2002). Within single plant types, root water uptake profiles vary with above-ground biomass and age, as larger and older trees tend to have deeper roots enabling them to tap deep moisture (Schenk and Jackson, 2002; Tao et al.,

2021). Furthermore, across similar climates, plant water uptake differs along topographic positions. Roots are shallower in uplands and lowlands, making vegetation more reliant on surface soil moisture, while roots go deeper in between these landscapes to benefit from the surface and deep moisture during seasonal wetting and drying (Fan et al., 2017).

Yet, the scientific consensus on the global relevance of surface and deep soil moisture for vegetation functioning is still lacking. Past studies,analyzing the role of soil moisture for vegetations show contrasting results, which might be because of disparities in data and methods employed. Feldman et al. (2022), with site-based isotope tracer studies, have emphasized the relevance of shallow soil moisture for most vegetation compared to deeper soil moisture, as water uptake preferentially takes place from the roots concentrated in the top few centimeters. Vegetation prefers shallow moisture to deep moisture owing to less energy expenditure in water uptake, higher nutrient concentration, and less oxygen deficiency on the surface (Schenk and Jackson, 2002). Similarly, gross primary productivity (GPP) is most related to 0-20 cm soil moisture in water-limited grassland ecosystems (Fang et al., 2018). In contrast, Miguez-Macho and Fan (2021) highlight vegetation's widespread dependence upon past precipitation stored in the deep soil globally, with the degree of dependence following climatic regimes and associated typical levels of water stress. The vegetation in semi-arid and seasonally arid climatic regions depends most on the deep water compared to other climatic zones. Moreover, the inter-annual carbon dioxide growth rate in the atmosphere correlates well with the total water storage anomalies on a global scale, implying the role of the overall water column in vegetation functioning (Humphrey et al., 2018).

The water uptake can further change during droughts. Studies show that the vegetation water uptake shifts to a deeper moisture layer during dry years to alleviate plant water stress and maintain transpiration (Migliavacca et al., 2009; Tao et al., 2021).). Also, it has been found that the typical water uptake depth differs along vegetation types during drought. For instance, grasses and herbaceous plants show increased sensitivity to surface soil moisture during the dry period (Geruo et al., 2017), making them highly susceptible to drought. Following surface moisture replenishment after drought due to a large precipitation event, grasses show greater resilience than trees as they recover faster (Yang et al., 2014), while the trees take time to shift water uptake between layers (Tao et al., 2021).

These past studies analyzing the relevance of surface and deep soil moisture are primarily focused on point or regional scale (Migliavacca et al., 2009; Tao et al., 2021; Yang et al., 2014; Fang et al., 2018; Geruo et al., 2017), lacking a comprehensive view of vegetation's reliance on soil moisture globally. Also, some studies, which focus on the role of surface and deep

soil moisture on vegetation, used reanalysis-based soil moisture estimates (Li et al., 2021; Miguez-Macho and Fan, 2021), whose results are likely to be impacted by the underlying model assumptions affecting estimated soil moisture dynamics, particularly for deeper layers where less observational constraints are available. Our study analyses the role of surface and deep soil moisture for vegetation functioning globally with satellite-based observational soil moisture datasets to overcome these shortcomings.

This thesis focuses on understanding the role of surface and deep soil moisture in vegetation functioning. Precisely, we study how the role of surface and deep soil moisture changes spatially across varying vegetation types and climatic regimes, and temporally during dry months. We calculate a correlation between Sun-induced fluorescence (SIF), a proxy for photosynthesis, with surface and deep soil moisture, to understand the role of soil moisture in vegetation functioning respectively. We utilize the European Space Agency Climate Change Initiative (ESA CCI) soil moisture dataset for surface soil moisture (SSM) and GRACE total water storage anomalies (TWSA) as an estimate for the deeper soil moisture. The correlation results are then presented for different vegetation and climate types. Furthermore, by calculating the correlation for the driest months, we study if plants shift to using deeper soil moisture layers during dry periods.

2 Objective of the study

This study focuses on understanding the roles of surface and deep soil moisture for global vegetation productivity. In this context, we correlate the monthly anomalies of surface and deep soil moisture, respectively, with vegetation photosynthesis activity in water-limited regimes. I explicitly focus on water limited regions because vegetation productivity does not follow water availability dynamics in energy-controlled regimes. In computing correlation globally, we aim to understand how this correlation varies with the surface and deep soil moisture in such water-limited conditions. The general objectives of this study are:

1. To determine the spatial and temporal occurrence of water limitation on vegetation functioning.

2. To understand the role of surface and deep soil moisture in vegetation photosynthesis.

3. To analyze how the relationship of vegetation photosynthesis with surface and deep soil moisture varies spatially across different vegetation types and climatic regimes.

4. To determine if plants shift to using deeper soil moisture during dry months. If yes, how does the root water uptake from deeper soil moisture vary with vegetation types and aridity?

3 Datasets

Table 3.1 Overview of datasets used in this study.

Datasets	Variables	Source	Time-period	References
Vegetation functioning	Sun-Induced Fluoroscence (SIF)	GOME-2	2007-2018	Köhler et al. (2015)
Soil Moisture	Surface Soil Moisture	ESA-CCI	1978-2021	Dorigo et al. (2017)
	Total Water Storage Anomalies (TWSA)	GRACE	2002-2018	(Landerer and Swenson, 2012)
	Multi-layered Soil Moisture (SoMo)	SoMo.ml	2002-2019	O and Orth (2021)
Climate	Temperature (T), Precipitation (P) and Radiation (R)	ERA-5	2000-2020	Hersbach et al. (2020)
Vegetation Class	Land Cover Data	IGBP	1982-2021	M.A. et al. (2010)
	Tree Cover Fraction	VCF5KYR	1982-2016	Hansen, M., Song, X. (2018)

3.1 Vegetation Functioning

The energy from sunlight triggers a light reaction in vegetation. The excess energy from photosynthetically active radiation (PAR), the spectral band of solar radiation (380-710 nm) that plants can use for photosynthesis, is dissipated by leaf either as chlorophyll fluorescence (CF) emission or lost through heat (Non-Photochemical Quenching (NPQ)) (Mohammed et al., 2019). Hence, the CF emission is directly related to the plant's photosynthetic machinery. The satellite-based hyperspectral resolution spectroradiometers receive these CF emissions, and retrieval methods further disentangle vegetation fluorescence signals from other sources such

as surface reflectance (Guanter et al., 2012). Since the reflected radiance by the vegetation is strongly retained within oxygen absorption zones or Fraunhofer lines due to the strong absorption of the incoming sunlight, it becomes possible to retrieve fluorescence emission from the signals captured by the satellite. Thus, the entire Sun-Induced Fluorescence (SIF) spectrum (650-800 nm) is then reconstructed from these fluorescence emissions exploiting the distinct absorption features in the red (R) and Near Infrared (NIR) spectral window (Berger et al., 2022). This SIF spectrum has two maxima under ambient temperature, one in R (685-690nm) (F685) and the other in the far-red spectral region (730-740nm) (F740) (Figure 3.1) (Mohammed et al., 2019).
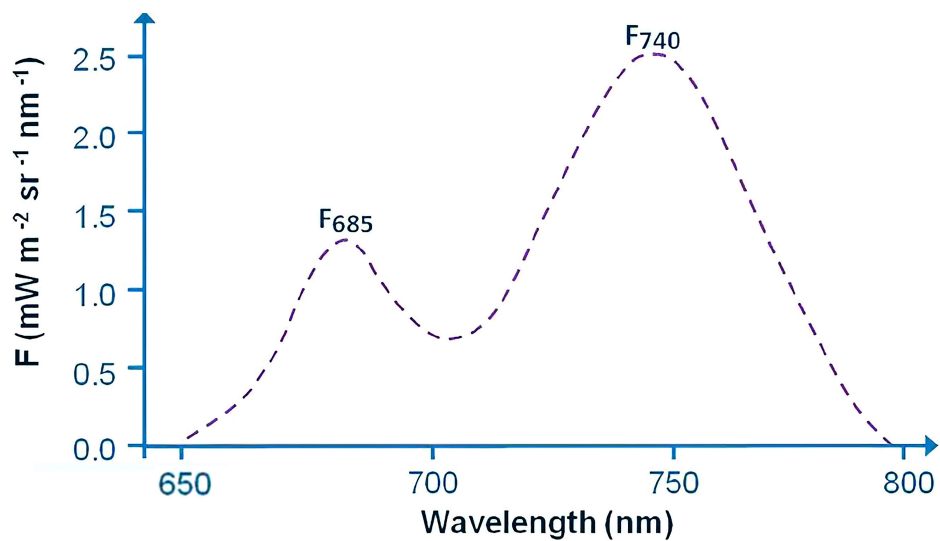
Figure 3.1: Conceptual figure of leaf fluorscence emission with maxima in the red and far-red spectral regions. Adopted from Mohammed et al. (2019)

The absorption, scattering, and re-absorption of the emitted SIF signal occur, depending upon canopy structural properties. The SIF retrieval methods correct this by determining the escape probability of the SIF signal to estimate canopy level SIF (Guanter et al., 2014). Additionally, the multiple environmental and atmospheric drivers affect the SIF signal before reaching the satellite sensor. Nevertheless, SIF is less affected by these drivers than vegetation indices like the Normalized Difference Vegetation Index (Guanter et al., 2015), making it a reliable proxy for vegetation functioning.

SIF data are increasingly used to track the photosynthetic dynamics in different ecosystems (Köhler et al., 2018; Walther et al., 2016, 2018; Ma et al., 2016). Moreover, SIF is used in studies related to the coupling of carbon and water fluxes at the regional scale, considering its close link with gross primary production (GPP) (Zhang et al., 2018; Koffi et al., 2015).SIF has been utilized to indicate drought and temperature stress at ecosystem scales (Zarco-

Tejada et al., 2009; Wang et al., 2018; Wu et al., 2018) and to identify hydrometeorological drivers of the global vegetation (Li et al., 2021). Among available observation-based global SIF products (Bandopadhyay et al., 2020),we considered the Global Ozone Monitoring Experiment's (GOME-2) SIF data in our study because it provides relatively reliable data over a long period (2007-2018). The revisiting time of the satellite carrying the GOME-2 instrument is eight days, while SIF estimates are derived for 16-day periods. The global raw SIF observations are processed to obtain monthly data at 0.5-degree spatial resolution as in Köhler et al. (2018) and can be accessed from `https://www.gfz-potsdam.de/sektion/fernerkundung-und-geoinformatik/projekte/global-monitoring-of-vegetation-fluorescence-globfluo/daten`.

3.2 Soil moisture

Soil moisture is the crucial variable controlling numerous processes and feedbacks in climate systems. It is generally defined as water contained in an unsaturated soil zone. It constrains plant transpiration and photosynthesis in water-limited regimes, thereby impacting global water, energy, and biogeochemical cycles (Seneviratne et al., 2010)

Global soil moisture datasets are obtained through different techniques that have their strengths and limitations. Though in situ measurements provide precise soil moisture information, they are difficult to set up and maintain globally. Consequently, they are limited in numbers and distributed non-uniformly throughout the globe, inhibiting the usage of ground-based soil moisture datasets in global-scale studies.

Satellite-based microwave remote sensing provided global observation of surface soil moisture using different passive and active remote sensing techniques. The recent advancements in remote sensing methods, retrieval algorithms, calibration, and validation techniques make satellite-based surface soil moisture suitable for the global study of soil moisture vegetation relationships. We use soil moisture data from the European Space Agency (ESA) Climate Change Initiative Program (CCI), which combines active and passive microwave measurement products to provide reliable estimates of surface soil moisture (SSM) (Dorigo et al., 2017). The ESA CCI soil moisture data is available from 1978 to 2021 at 0.25 degrees spatial and daily temporal resolution and be accessed through `https://esa-soilmoisture-cci.org/`.Since microwave remote sensing fails to give reliable estimates in areas with dense vegetation (tropical and boreal forests), mountains (Himalayas), ice cover (Greenland, Antarctica), and deserts, these areas have been masked out in the original ESA CCI soil moisture dataset.

The surface soil moisture estimate from microwave remote sensing may not fully represent the root zone soil moisture available for the vegetation as it represents only the top centimeters of soil into which the microwave radiation can propagate. Furthermore, the surface and deep soil moisture get decoupled during the dry period, making microwave observations less representative of the root zone soil moisture during such periods (Capehart and Carlson, 1997). Soil moisture data simulated by land surface models (LSMs) is an alternative, providing global soil moisture at different depths. However, LSM outputs are prone to uncertainties in (i) the meteorological forcing data, (ii) inaccurate knowledge of soil and vegetation characteristics, and (iii) uncertainties in the representation of complex processes such as photosynthesis, infiltration, or evaporation (Koster et al., 2009; Seneviratne et al., 2010).

The Gravity Recovery and Climate Experiment (GRACE) satellite, launched in 2002, offers the possibility of studying the relationship between vegetation and the total water column. GRACE provides monthly terrestrial water storage anomalies (TWSA) by measuring Earth's gravity field changes (Landerer and Swenson, 2012). The TWSA includes water storage anomalies of snow, canopy water, surface water, soil water, and groundwater. Though available only at a relatively coarse resolution of 300 km, GRACE TWSA has been used successfully to study vegetation moisture relationships (Yang et al., 2014; Geruo et al., 2017; Chen et al., 2022). We use the JPL-Mascons product from `https://podaac.jpl.nasa.gov/dataset/TELLUS_GRAC-GRFO_MASCON_CRI_GRID_RL06_V2` , which is available at a monthly temporal resolution from April 2002 to the present and a spatial resolution of $0.5° \times 0.5°$ degrees. TWSA has been successfully utilized as an indicator of water availability to study vegetation moisture relationships on a regional (Chen et al., 2022; Andrew et al., 2017) and global scale (Xie et al., 2019).

The two datasets, ESA CCI SSM and GRACE TWSA hint at the relevance of surface and deep moisture layers for vegetation but do not allow a fair comparison of relevance between layers because of the different noise levels in these datasets. Besides observational estimates of soil moisture to study how vegetation functioning relates to the surface and deep soil moisture, we employ machine learning-based soil moisture estimates SoMo.ml (O and Orth, 2021). A Long Short-Term Memory (LSTM) model has been trained using in-situ soil moisture to obtain the multilayer SoMo dataset (0-10 cm, 10-30 cm, and 30-50 cm) at 0.25 degrees spatial and daily temporal resolution from 2000 to 2019. Since the three SoMo layers have similar noise levels, the results obtained using the SoMo dataset facilitates the intercomparison of correlation between layers and help us to validate the results from the SSM and TWSA datasets independent of the way soil moisture data is obtained.

3.3 Climate and Vegetation Data

Employed climate variables include daily air temperature (T), precipitation (P), and net radiation (R) from the ERA5 renanalysis products, which can be accessed from `https://www.ecmwf.int/en/forecasts/datasets/reanalysis-datasets/era5` . T and R are used as the control variable for computing the partial correlation of SIF with soil moisture as these energy variables likely confound the SIF-soil moisture correlation. The correlation results are compared for different aridity types for which I compute the aridity index as the ratio between the long-term mean of R (mm) (1 MJ/sq.m/day = 0.408 mm/day) and P (mm) for each grid cell (Budyko1974).

To study the variation of correlation between SIF and soil moisture across vegetation types, we incorporate land cover classifications from the International Geosphere-Biosphere Programme (IGBP) dataset, accessed through `https://climatedataguide.ucar.edu/climate-data/ceres-igbp-land-classification` and tree cover fraction data from the Vegetation Continuous Fields (VCF5KYR) Version 1 data product , accessed from `https://lpdaac.usgs.gov/products/vcf5kyrv001/` . These two datasets are obtained independently and facilitate the intercomparison and validation of the correlation pattern obtained across vegetation types.

4 Methodology

```
┌─────────────────────────────────────┐
│                                      │
│    Timeseries of TWSA,SSM,SIF,T,R    │
│                                      │
└─────────────────────────────────────┘
                    │
                    ▼
┌─────────────────────────────────────┐
│  Deseasonalize and detrend time se-  │
│  ries. (only if linear trends are present.) │
└─────────────────────────────────────┘
                    │
                    ▼
┌─────────────────────────────────────┐
│                                      │
│  • Filter for growing season/sparse vege- │
│    tation ($SIF > 0.5$)              │
│                                      │
│  • Filter for months, where observation of │
│    SSM, TWSA and SIF are not available. │
│                                      │
│  • Filter for removing effect of frozen soil │
│    moisture. ($T < 5°C$)             │
│                                      │
└─────────────────────────────────────┘
                    │
                    ▼
┌─────────────────────────────────────┐
│  If no of observations for a grid    │
│  cell are greater than 40, then      │
│                                      │
│  • Compute partial correlation between │
│    SIF and SSM, r(SIF  ∼  SSM), after │
│    controlling effects of T and R.   │
│                                      │
│  • Compute partial correlation between │
│    SIF and TWSA, r(SIF  ∼  TWSA), after │
│    controlling effects of SSM, T and R. │
└─────────────────────────────────────┘
```
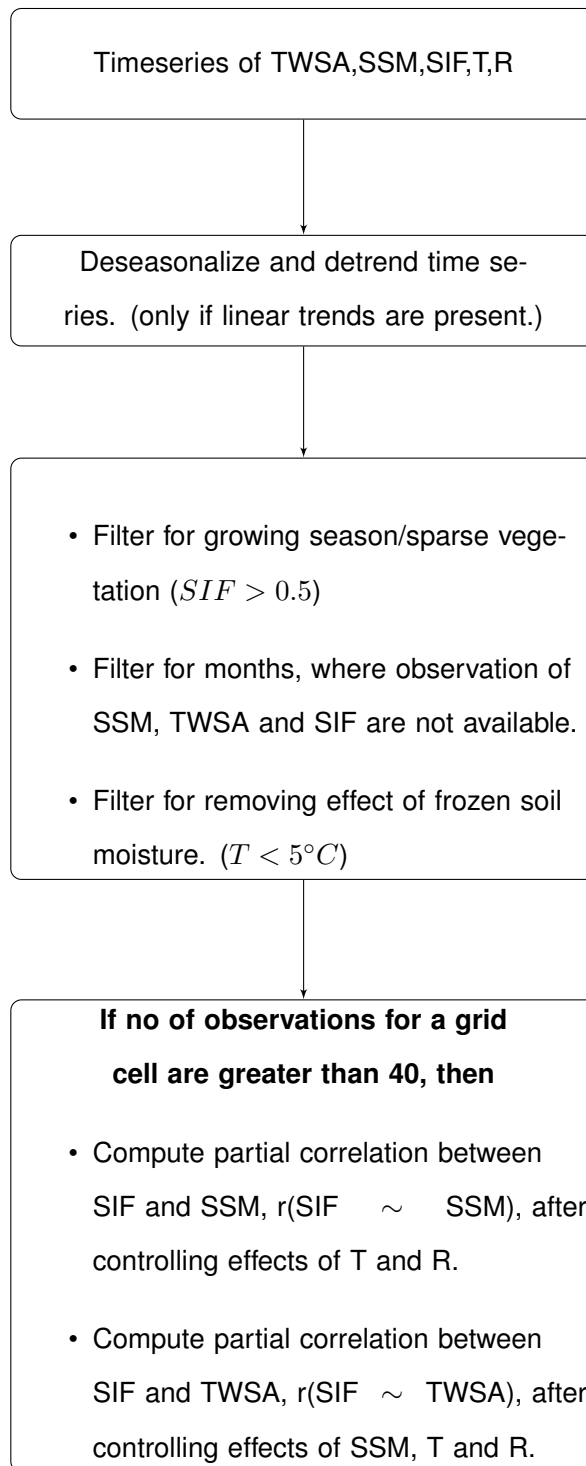
Figure 4.1: Flowchart showing data processing and analyzing steps.

The flow chart of overall data processing and analysis is presented in Figure 4.1. All datasets are available at a common 0.5 x 0.5-degree spatial resolution and monthly temporal resolution.

The time period of analysis is from 2007 to 2018 constrained by the concurrent availability of all involved datasets. The monthly anomalies are calculated by subtracting the longterm mean monthly cycle and removing the linear trend if any significant ($p < 0.05$). SIF and T thresholds are applied in each grid cell to filter out non-growing season data. This allow our analysis to focus on vegetation-soil moisture relationships in growing months. For this purpose, we filter out months when the absolute SIF value is less than the threshold of 0.5 $mW/m^2/sr/nm$ to focus on months with significant vegetation activity. We apply an additional temperature threshold ($T > 5°C$) to remove the months with frozen soil, similar to (Li et al., 2021). We do not consider months during which either soil moisture or vegetation functioning records are unavailable or filtered out.

Then, the correlation between SIF and soil moisture is calculated for a grid cell when observations for at least 40 months are present after filtering. T and R might also be affecting SIF in addition to soil moisture. To focus exclusively on the effects of water availability on SIF, we correct the confounding effects of T and R by calculating partial correlations between SIF and SSM, r(SIF $\sim$ SSM), while accounting for T and R. The partial correlation calculates the degree of association between two variables, removing the effect of a set of confounding variables. The same is done in the case of TWSA where we further remove the impact of SSM on TWSA to better isolate the deep soil moisture dynamics by computing the partial correlation of SIF with deep soil moisture, r(SIF $\sim$ TWSA), while accounting for T, R and SSM. Since we focus on understanding the role of soil moisture on vegetation photosynthesis, which is primarily critical in water-limited conditions, we remove the grids cells with negative correlation, r(SIF $\sim$ SSM) or r(SIF $\sim$ TWSA), from our analysis. Such negative correlation indicate that soil moisture is not a limiting factor for the vegetation and may hint at vegetation's converse effect on soil moisture (increasing vegetation activity causing depletion of soil moisture). Additionally, a negative correlation occurs in the grid cells where water limits vegetation productivity through oxygen limitation.

We also calculate the partial correlations separately with only considering dry months in each grid cell. We determine the dry months as the months with the fifteen lowest absolute values of TWSA for which SIF and soil moisture data are available. In the analyses for dry months, we exclude grid cells with less than 60 observations, so that the dry months represent the driest 25 percent of the data or less. Precisely, these are the driest months in which vegetation is still photosynthesizing since we remove the months with no vegetation activity with a threshold of $SIF < 0.5$. Furthermore, to determine dry months, we use TWSA values as it is the overall indicator of the total water column rather than surface soil moisture, which only represents the top few centimeters of the soil. Besides, TWSA has been widely used to identify extreme

droughts in different parts of the world (Chen et al., 2010; Houborg et al., 2012; Ma and CCI SM in Yunnan Province, 2017; Yirdaw et al., 2008). Nevertheless, the driest 15 months may not represent similar extremeness globally. For instance, the degree of dryness for a grid cell with 144 observations $(15/144)$ and the grid cell with only 60 observations $(15/60)$ after filtering would be different, the latter likely to be less extreme than the former.

In order to analyse the global correlation results, we group the grid cells with respect to aridity and tree cover/ land cover classes. Each grid cell is assigned the dominant vegetation types on analyzing correlation results. Afterward, the mean correlation of SIF with soil moisture estimates is calculated for each group if more than 20 grid cells are available. Then we anlayse the evolution of r(SIF $\sim$ SSM) and r(SIF $\sim$ TWSA) across aridity and vegetation classes.

5 Results and Discussion

5.1 Global Patterns of water limitation on vegetation

The partial correlation between SIF and soil moisture allows for determining the extent of water-limited areas globally. In the growing season, SIF correlates positively with soil moisture (both r(SIF $\sim$ SSM) and r(SIF $\sim$ TWSA)) in approximately forty percent of our global study area, indicating water limitation on vegetation (Figure 5.1a). The actual extent of water limitation on vegetation globally is greater than forty percent because our filter criteria remove arid regions (Sahara, Australia, and Central Asia), which are typically water limited, from the analysis. This estimate, excluding arid regions, aligns with previous estimates that approximately half of the global land area is water-limited (Heimann and Reichstein, 2008; Dirmeyer et al., 2006). Vice versa, a negative correlation between vegetation and soil moisture is present in boreal forest regions in high latitudes, the eastern United States, and Northern Europe. The negative correlation, r(SIF $\sim$ SSM) or r(SIF $\sim$ TWSA), arises if excess vegetation activity causes soil moisture depletion or excess water impacts vegetation activity, possibly through water logging by oxygen limitation.

The continental pattern of water limitation on vegetation, calculated with the correlation of SIF and soil moisture anomalies, agrees well with spatial patterns of the evapotranspiration regimes (water or energy limitations) identified using the FLUXNET measurements in Europe and North America (Teuling et al., 2009). The FLUXNET provides direct and continuous eddy covariance flux measurements of evapotranspiration (ET) and global radiation (Rg) from different sites across varying climate and vegetation zones (Baldocchi et al., 2001). The global patterns also align with the yearly correlation of evapotranspiration with global radiation (energy) and precipitation (water) calculated using LSM data from the Global Soil Wetness Project where models were driven with observation-based meteorological forcing (GSWP) (Dirmeyer et al., 2006).These past studies incorporate different data sources in their study compared to ours, yet the global patterns of water limitation on vegetation obtained here are similar to them, ensuring the validation of derived global patterns. For further results, I focus on water-limited regions (with positive r(SIF $\sim$ SSM) and r(SIF $\sim$ TWSA)) only, because the role of soil moisture in vegetation photosynthesis is only critical in water-limited conditions.
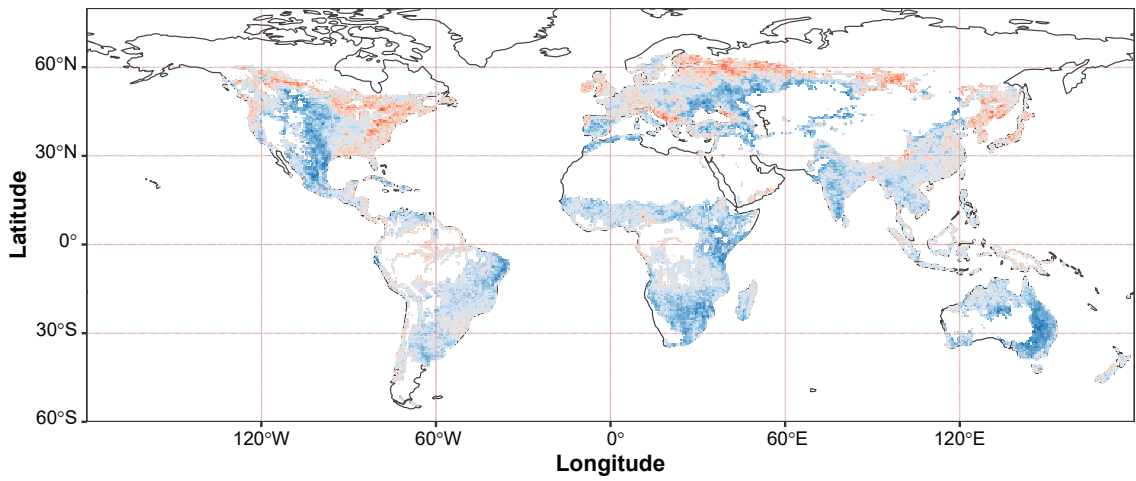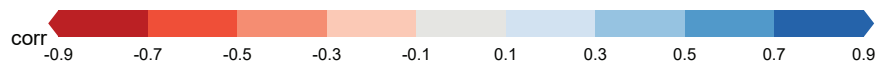
(a)
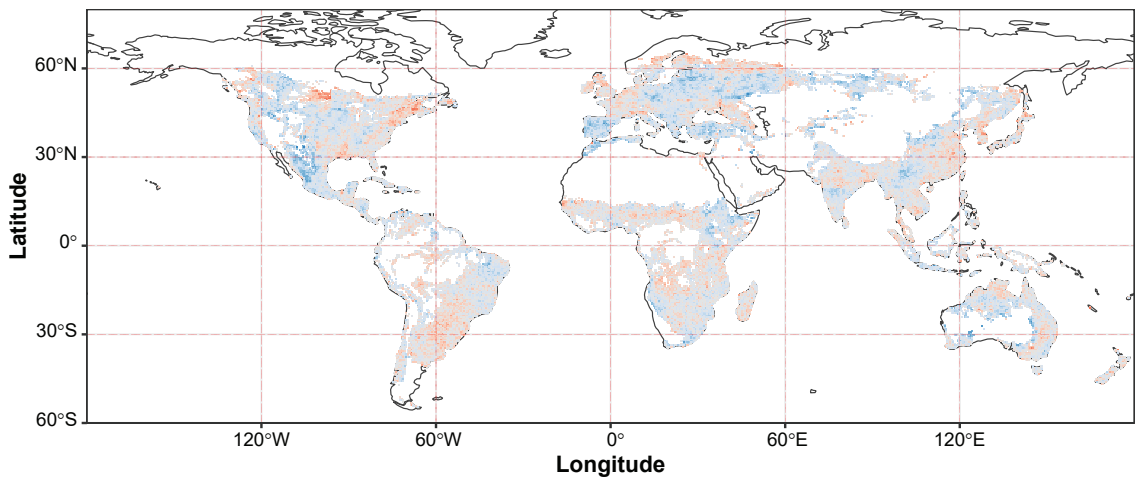
(b)

Figure 5.1: Partial correlation of SIF with (a) surface and (b) deep soil moisture for growing season months. Positive value (blue) indicates that the vegetation functioning is water limited while negative value (red) indicates that water availability does not impact the vegetation functioning. The grids present in the land-mass, which are filtered out, do not have any color.

5.2 Correlation of vegetation photosynthesis with surface and deep soil moisture in water-limited regions during growing months

The partial correlation of SIF with surface soil moisture varies globally (Figure 5.2a). SIF correlates strongly with surface soil moisture in semi-arid climates, which include shrublands in Central North America (NA), Savannahs in South America (SA) and Africa, and grasslands in South Africa and Australia in growing season months. The r(SIF $\sim$ SSM) correlation is stronger in Southern Europe (SE) and the Mediterranean region compared to central and Northern Europe (NE). The gradient of correlation (r(SIF $\sim$ SSM)) from the hot and dry Mediterranean region to wet and cold NE is similar to the gradient of drivers of evapotranspiration regimes (water limitation in the SE to energy limitation in the NE) obtained in other studies (Denissen et al., 2022; Teuling et al., 2009). Stronger correlations between SIF and surface soil moisture are also found in the croplands: the area around the Black Sea, part of Eurasia, and South India. Studies show that the crops typically draw water from the soil in the upper layer, and water uptake decreases with increasing soil depth (Feldman et al., 2022). Though these croplands are not heavily irrigated areas, obtained from Global Map of Irrigation Areas Version 4 (https://www.fao.org/land-water/resources/graphs-and-maps/details/en/c/237286/) , the correlation value is likely to be affected by any crop water management practice.

The r(SIF $\sim$ TWSA) correlation roughly follows a similar pattern of r(SIF $\sim$ SSM) globally (Figure 5.2b). The partial correlation of SIF with deep soil moisture is higher in drier central NA and SE compared to other regions. The deeper soil moisture is coupled to surface soil moisture through infiltration and capillary rise. During precipitation-rich periods, infiltration dominates and leads to strong coupling, while during drier periods evapotranspiration tends to remove moisture preferentially from the upper soil leading to a decoupling of the shallow and deeper soil moisture if this cannot be compensated by capillary rise. Hence, the similarity in the global pattern of correlations of vegetation functioning with surface and sub-surface soil moisture during the growing season months, which includes both dry and wet months, is expected. The global correlation pattern of SIF with deep soil moisture,r(SIF $\sim$ TWSA), is similar to the correlation between TWSA and the normalized difference vegetation index (NDVI), obtained in the study by (Yang et al., 2014). Yet, we obtain smaller correlation strength between SIF and TWSA compared to the correlation of NDVI with TWSA in Yang et al. (2014), which could stem from the difference in methodology between these studies. We filter out the effect

of surface soil moisture in the correlation of SIF with TWSA using partial correlations, while (Yang et al., 2014) calculated the correlation of NDVI with the whole water column present in TWSA, which includes surface soil moisture. Furthermore, (Yang et al., 2014) did not control for the confounding effects of temperature and radiation on soil moisture availability, affecting the correlation r(NDVI $\sim$ TWSA), particularly in energy-controlled areas.

For two-thirds of water-limited regions (positive correlation of SIF with both SSM and TWSA), the correlation r(SIF $\sim$ SSM) is greater than r(SIF $\sim$ TWSA) (Figure 5.2c). This stronger correlation with surface soil moisture is in line with the findings of several studies that plants usually extract water from the surface soil moisture (Feldman et al., 2022; Fang et al., 2018; Geruo et al., 2017) owing to less energy expenditure in plant water uptake, nutrient availability, and ample supply of oxygen. Nevertheless, the difference between r(SIF $\sim$ SSM) and r(SIF $\sim$ TWSA) is not uniform globally. Greater differences are found in semi-arid climates in central NA, Australia, African grasslands, and Eurasian croplands, with r(SIF $\sim$ SSM) being relatively higher than r(SIF $\sim$ TWSA). In contrast, in the temperate dry SE and moist NE and some regions of western NA, the correlation of SIF with deep moisture is almost similar or even greater than the correlation with SSM, implying comparable or greater influences of sub-surface soil moisture on vegetation functioning in growing season months.
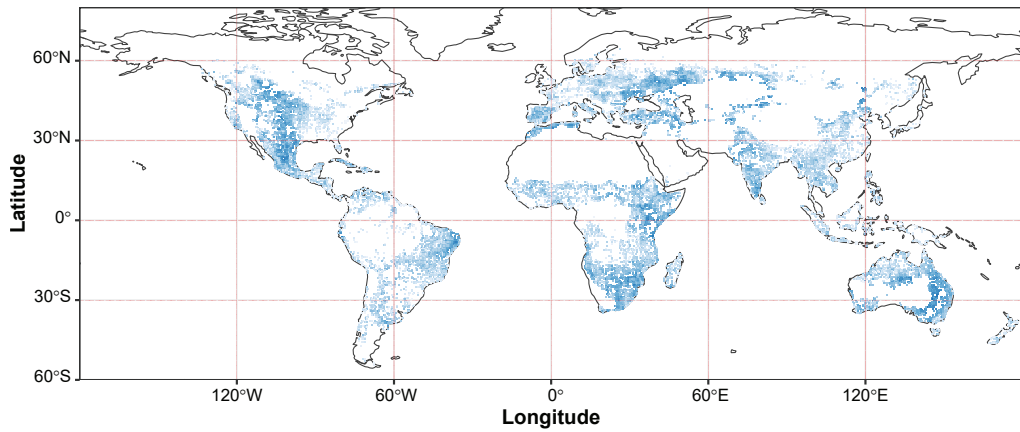
(a)
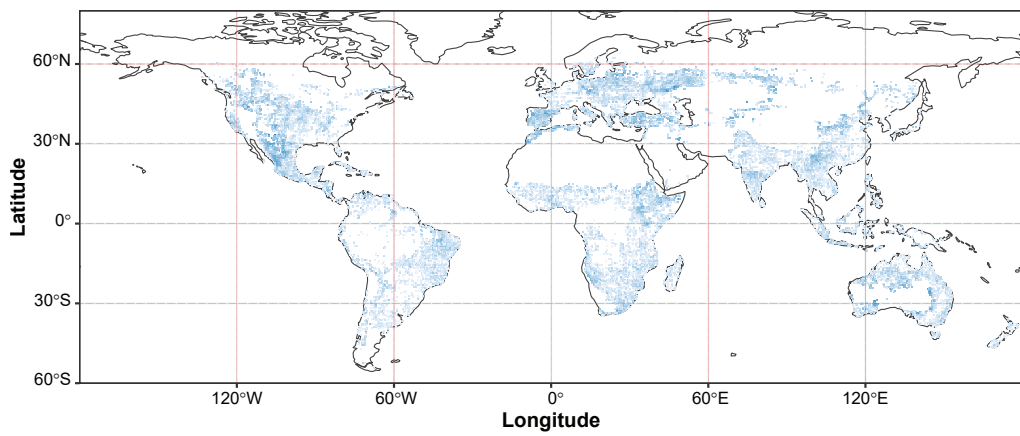
(b)
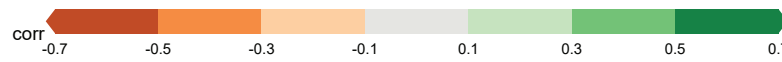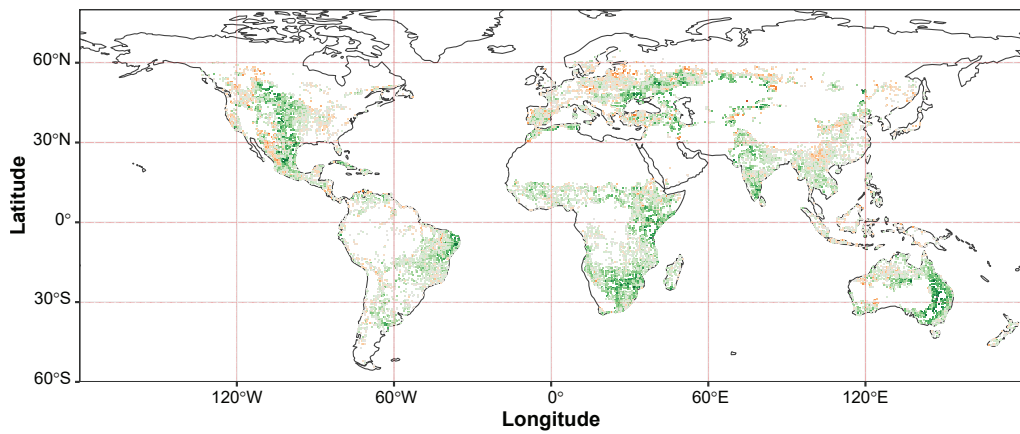
(c)

Figure 5.2: The partial correlation of SIF with (a) surface soil moisture and (b) deep soil moisture and (c) the difference between the surface and deep soil moisture [a-b].

5.3 The correlation of vegetation functioning and soil moisture for the vegetation types.
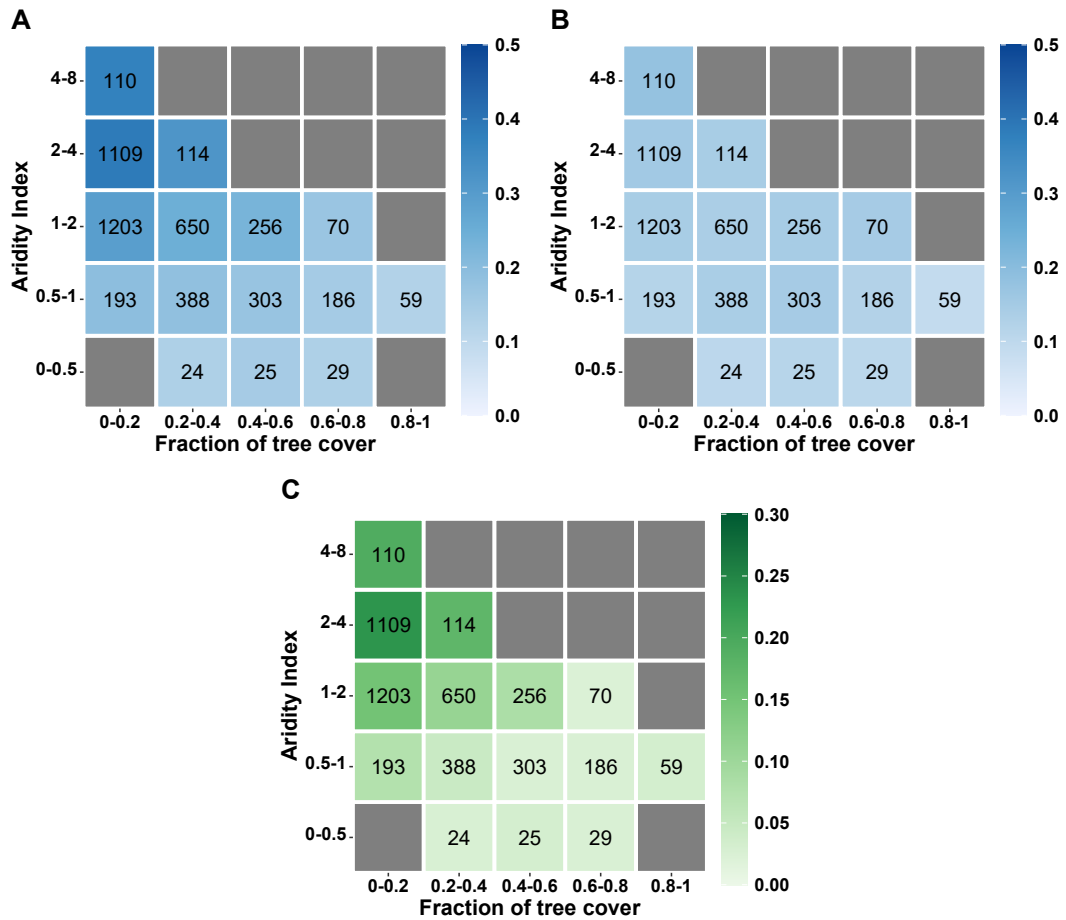

Figure 5.3: Partial correlation of SIF(a) r(SIF ~ SSM), (b) r(SIF ~ TWSA), and (c) difference (A-B) in growing months for varying tree cover fraction and aridity index. The gray regions denote the classes where sufficient grid cells (no of grid cells ≥ 20) are not available. To compute this, each grid cell is assigned an aridity index and tree cover fractions. Then, the partial correlations are averaged across grid cells with similar climate and vegetation characteristics. The number in each box denotes the number of grid-cells available within the respective climate-vegetation regime.

The partial correlation between SIF and surface soil moisture varies along tree cover fractions with stronger correlations for low tree cover fractions (Figure 5.3a). Regions with low tree cover fraction could be dominated by e.g. grasses, crops, or shrubs which typically have the majority of their roots in the upper soil. This negative gradient along tree cover fractions is more pronounced in semi-arid to arid regions (AI in the range 1-4) than in humid regions (AI < 1). We compare the partial correlation across different land cover types from the IGBP

dataset, which is independent of the tree cover fraction dataset.Yet, the comparison of correlation across different land cover types (Table 5.1a) also confirms that the grasslands (r= 0.34), savannas (r = 0.33), and shrublands (r = 0.34), which have low tree cover fractions, are strongly correlated with surface soil moisture compared to the forest of all types (r = 0.15, range of 0.09 – 0.22) during growing months. Despite varying tree cover fractions, we could not observe a difference in the correlation of SIF with SSM in very wet regions in growing months in Figure 5.3a. This is because wet regions typically have ample moisture supply for vegetation, decreasing the sensitivity of vegetation functioning to surface soil moisture fluctuations.

The partial correlation between SIF and TWSA is similar for all land cover types (Table 5.1b) and tree cover fractions (Figure 5.3b) for the growing months.We do not find a gradient in the correlation along the land cover types, in contrast to several other studies analyzing vegetation TWSA relationships. The TWSA $\sim$ NDVI interaction is found to be stronger in grasslands, followed by shrublands, savannahs, and forests in Australia (Yang et al., 2014; Geruo et al., 2017; Chen et al., 2022) and globally (Xie et al., 2019). However, all these studies focused on the overall water column (including surface soil moisture) for estimating TWSA $\sim$ NDVI interaction, while in this study, we control for the effect of surface soil moisture in analyzing the SIF $\sim$ TWSA relationship. Since, in the non-dry period, the TWSA and SSM are highly correlated (Figure C.6) , a high correlation between vegetation functioning and TWSA might occur because of the high correlation between vegetation functioning and SSM, which is included in TWSA.

Table 5.1 Partial correlation of SIF with (a) surface and (b) deep soil moisture along varying land cover class and aridity index in growing season months. For calculating this, each grid cell was assigned to the dominant vegetation type and aridity index. Then, mean correlations are calculated if each vegetation-climate class contains more than 20 grid cells.

(a)

Land Cover Types	Aridity Index				
	0-0.5	0.5-1	1-2	2-4	4-8
Evergreen Needleleaf Forest	-	0.09	0.13	-	-
Evergreen Broadleaf Forest	0.13	0.15	0.22	-	-
Deciduous Broadleaf Forest	-	-	0.20	-	-
Mixed Forest	0.13	0.15	0.16	-	-
Open Shrublands	-	-	0.27	0.36	0.38
Woody Savannas	-	0.21	0.24	0.38	-
Savannas	-	0.22	0.25	0.37	0.44
Grasslands	-	0.18	0.33	0.42	0.44
Croplands	-	0.17	0.29	0.38	0.30

(b)

Land Cover Types	Aridity Index				
	0-0.5	0.5-1	1-2	2-4	4-8
Evergreen Needleleaf Forest	-	0.16	0.18	-	-
Evergreen Broadleaf Forest	0.10	0.11	0.12	-	-
Deciduous Broadleaf Forest	-	-	0.14	-	-
Mixed Forest	0.12	0.14	0.18	-	-
Open Shrublands	-	-	0.19	0.17	0.20
Woody Savannas	-	0.13	0.12	0.15	-
Savannas	-	0.10	0.11	0.12	0.18
Grasslands	-	0.10	0.16	0.18	0.14
Croplands	-	0.14	0.12	0.13	0.16

The surface soil moisture is relatively more important than deep soil moisture in regions with low tree cover (Figure 5.3c). Grasslands and shrublands with low tree cover fractions rely highly on surface soil moisture, while forests with high tree cover fractions rely almost equally on the surface and sub-surface soil moisture. Forests generally have roots distributed across

larger depths, making them less vulnerable to surface soil moisture variations compared to grasslands typically with shallow roots, which are highly vulnerable to surface soil moisture fluctuations. Additionally, within the forest types, we find that needleleaf forests tend to use more water from deeper rather than shallow layers, while the opposite is found for broadleaf forests.

Grasslands' high sensitivity to surface soil moisture fluctuations is noted in multiple studies (Schenk and Jackson, 2002; Geruo et al., 2017; Fang et al., 2018). Fang et al. (2018) found that Gross Primary Productivity (GPP) is more responsive to surface soil moisture fluctuations in the surface layer (0-20 cm depth) than deeper layers (>20 cm) in grasslands in Inner Mongolia. Similarly, SIF's correlation with SSM is higher for grasslands compared to forests in Texas during both dry and wet months (Geruo et al., 2017). A particular exception, Li et al. (2021), identified that the soil moisture layer (7-28cm), not the layer (0-7) cm, primarily controls vegetation with low tree covers (grasslands and shrublands). Though our study does not disintegrate the soil moisture vertically in different depths comparable to Li et al. (2021), the discrepancies might stem from using different soil moisture datasets. Here, we use an observational soil moisture dataset, while Li et al. (2021) used a reanalysis-based ERA5 soil moisture dataset to train random forest models to identify the relative importance of different soil moisture layers on vegetation. The model-based soil moisture dataset inherently incorporates potentially inaccurate vegetation information used in the model simulations, thus impacting the resulting vegetation-soil moisture relationship determined from such soil moisture data (Koster et al., 2009).

5.4 The correlation of vegetation functioning and soil moisture for different aridity classes.

The partial correlation of SIF with SSM increases with an increase in the aridity index for all tree cover fraction classes (Figure 5.3a). This means vegetation photosynthesis in drier regions is more sensitive to surface soil moisture fluctuations than in wet regions. Also for a given land cover class, the partial correlation (SIF $\sim$ SSM) increases with increasing aridity (Table 5.1a). For instance, SIF's correlation with SSM are higher in drier grasslands (r(SIF $\sim$ SSM = 0.43)) than in wetter grasslands (r(SIF $\sim$ SSM = 0.18)) . Apart from grasslands, such an increasing correlation with the increase in aridity is distinct in shrublands, savannahs, and croplands. In drier regions, a lack of soil moisture limits vegetation photosynthesis and related transpiration. This is not the case for forests, typically found in humid regions, where the correlation between productivity and soil moisture does not vary with aridity.

By contrast, the correlation of SIF with deep soil moisture does not systematically change along aridity gradients for varying tree cover fractions and land cover types during the growing season (Figure 5.3b)(Table 5.1b). This similarity in r(SIF $\sim$ TWSA) with increasing aridity differs from the finding of Miguez-Macho and Fan (2021), who find that the vegetation dependence on past precipitation, stored in sub-surface soil moisture, is higher in semi-arid and seasonal-arid climates compared to humid. This difference in the relevance of deep moisture in semi-arid regions might stem from using different data sources. Miguez-Macho and Fan (2021) fused soil moisture and groundwater from the atmospheric reanalysis products, which are based on models with potentially inaccurate representations of land-atmosphere interactions as mentioned above. Here, we use an observational product to estimate deep soil moisture, which includes the water column beneath the surface layer and extending beyond the root zone. The TWSA considered here also includes the water in the deep aquifer, which is generally unavailable for vegetation. This large extent of deep soil moisture in our study compared to Miguez-Macho and Fan (2021) might also obscure the gradient of r(SIF $\sim$ TWSA) along aridity classes.

Vegetation photosynthesis correlates more stronger with surface soil moisture than deep soil moisture for all aridity classes (Figure 5.3c). Other studies also show that abundant nutrients, efficiency in water uptake, and fewer chances of root water logging aid plants to rely upon surface soil moisture whenever available (Schenk and Jackson, 2002; Feldman et al., 2022; Tao et al., 2021; Geruo et al., 2017). However, the difference in the correlation strength between surface and deep soil moisture (r(SIF $\sim$ SSM) - r(SIF $\sim$ TWSA)) is not uniform globally, with

drier regions having a greater difference in correlation compared to wetter. Increasing water limitation with increasing aridity makes photosynthesis more sensitive to surface soil moisture fluctuations, thereby increasing $(r(\text{SIF} \sim \text{SSM}))$. In contrast, increasing aridity does not seem to increase the correlation with deep soil $r(\text{SIF} \sim \text{TWSA})$. Thus, the difference in correlation, $(r(\text{SIF} \sim \text{SSM})$ - r(SIF $\sim$ TWSA)) mostly follows patterns of correlations of SIF with SSM, which is prominent in arid regions compared to humid.

5.5 Sensitivity of vegetation to the surface and deep soil moisture during dry months

The partial correlation between SIF and soil moisture is calculated separately for the driest 15 months. Since we focus on water-limited conditions only, the grid cells where the partial correlation between SIF and soil moisture is positive during both all growing-season months and the driest 15 months are included in this analysis.

The partial correlation between SIF and both surface and deep soil moisture increases during dry months (Figure 5.4)(Figure 5.5). Two-thirds of the vegetation area, water-limited in both growing and dry months (Figure 5.4c), shows an increase in correlation with surface soil moisture, while three-fourths of the such area shows an increase in correlation of SIF with deep soil moisture in dry months (Figure 5.5c). With the decrease in soil moisture, the water limitation on vegetation strengthens. Hence, photosynthesis in vegetation becomes more sensitive to the surface and sub-surface soil moisture variations in dry months compared to all growing season months. However, the partial correlation r(SIF $\sim$ SSM) decreases in some parts of central North America, Southern Europe, the Mediterranean, and Australia during drier months compared to all growing months. At the same time, these semi-arid regions experience a slight increase in the correlation of SIF with TWSA.

The correlation of SIF with surface soil moisture increases during drier months for all tree cover fractions and aridity classes (Figure 5.6a)(Table 5.2a). Water limitation on vegetation increases in dry months; hence, the surface soil moisture becomes critical for photosynthesis, irrespective of vegetation type. During the hydrological drought in Texas in 2011, the correlation of SIF with surface soil moisture varied, depending upon the vegetation types. The partial correlation r(SIF $\sim$ SSM) increased in grassland and forests, but decreased in shrublands (Geruo et al., 2017), while in this study I do not find varying responses across vegetation types in dry months. This discrepancy might have occurred from the dry month's definition, as the fifteen driest months represent different strengths of dryness in different regions. Thus, results obtained from local scale drought analysis (Geruo et al., 2017) might differ from this global scale analysis. Moreover, the increment in correlation r(SIF $\sim$ SSM) in dry months is higher in magnitude for humid regions compared to arid. Vegetation in arid areas is already exposed to water limitations in non-dry months; hence a comparatively minor increase in the correlation r(SIF $\sim$ SSM) occurs in dry months in arid regions compared to humid, which typically do not suffer water limitations.

Vegetation functioning correlates more strongly with deep soil moisture in dry months compared to all growing season months. This increase in correlation in dry months is consistent across tree cover fractions, land cover types, and aridity classes (Figure 5.5c)(Table 5.2b).A similar increase in correlation with TWSA during dry months was noted in grasslands and forests in Texas drought in 2011 (Geruo et al., 2017).Also, Miguez-Macho and Fan (2021) find that vegetation dependence on deep soil layers during dry months is higher in arid regions compared to humid regions. However, we do not find such an increase in correlation of r(SIF $\sim$ TWSA) with an increase in aridity in dry months. This difference might have stemmed from the incorporation of different datasets involved in analysis and the difference in analysis technique. Miguez-Macho and Fan (2021)) incorporated reanalysis-based datasets to get soil water profiles at different depths and used inverse modeling to predict root water uptake from different layers, while we incorporate observational-based soil moisture data and correlate it with SIF during the driest months to check if the vegetation dependence on the deep soil moisture increases along with an increase in aridity.
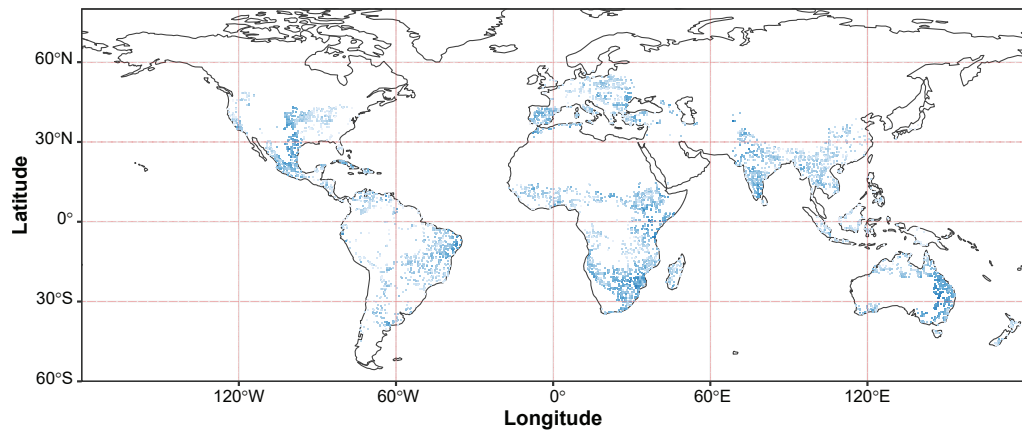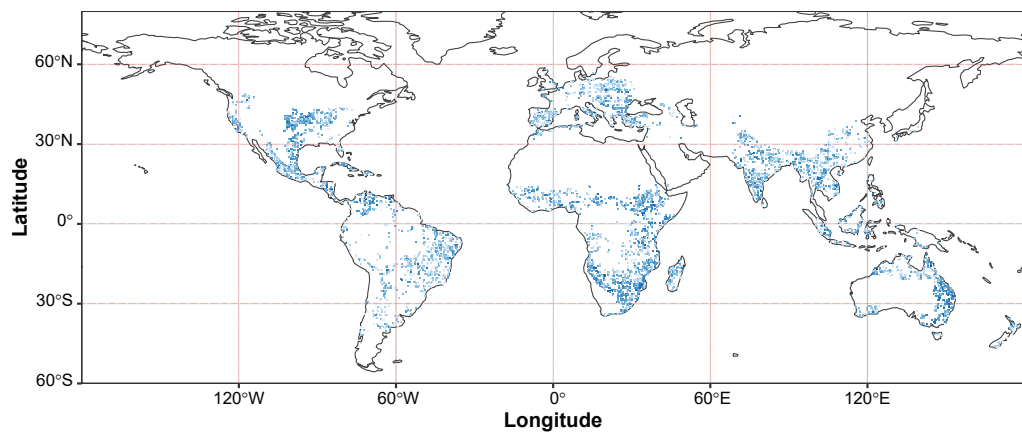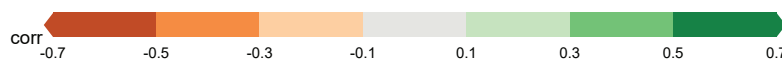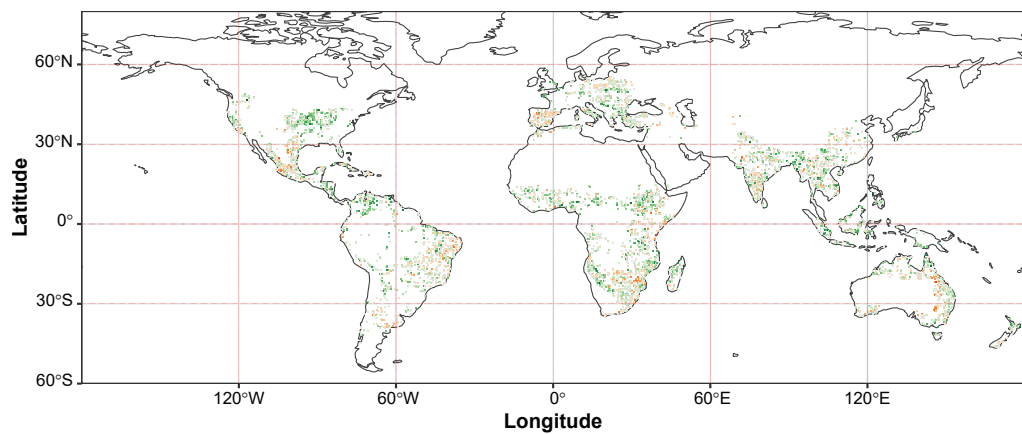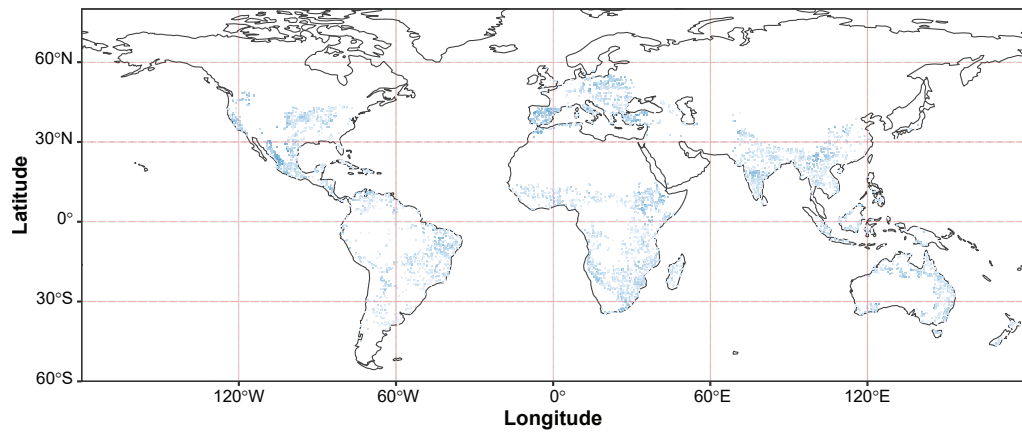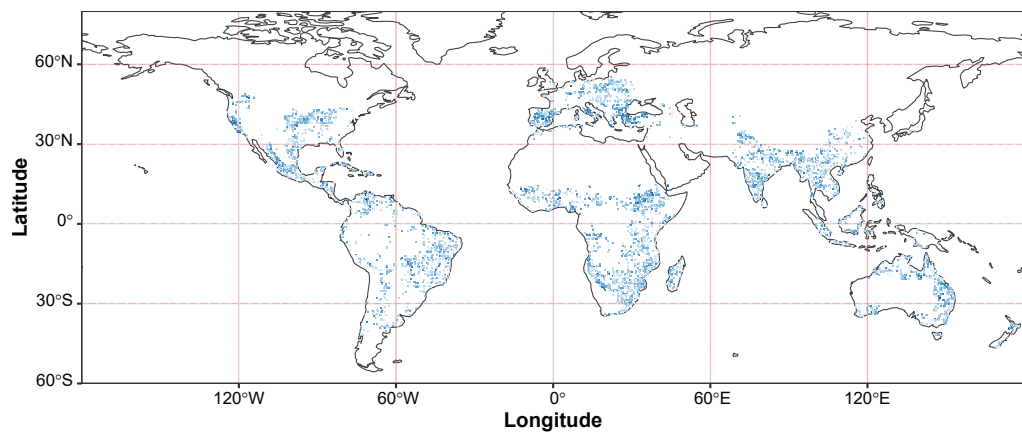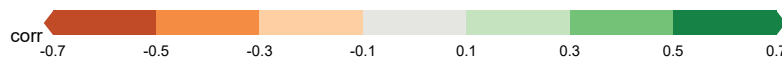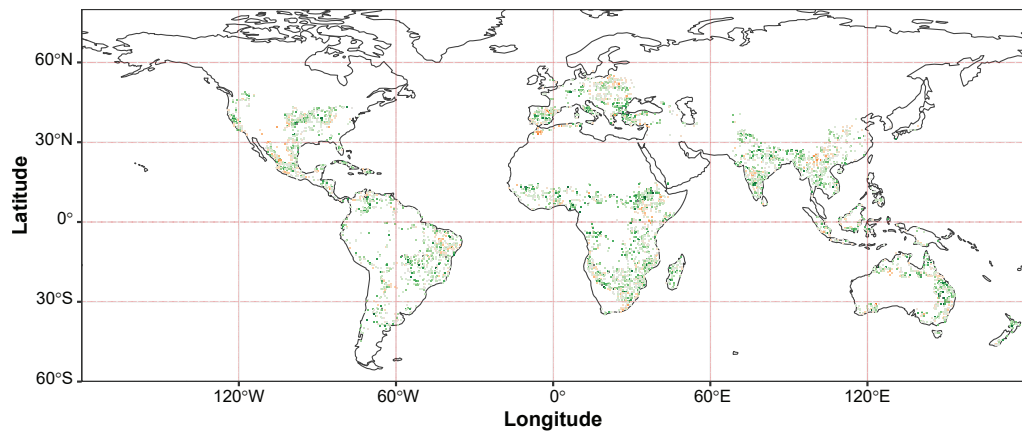
Figure 5.4: Partial correlation of SIF with surface soil moisture in (a) driest and (b) growing season months and (c) difference between driest and growing season months [a-b].

Figure 5.5: Partial correlation of SIF with deep soil moisture in (a) driest and (b) all growing season months and (c) difference between driest and growing season months [a-b].

Figure 5.6: Partial correlation of SIF with surface soil moisture in (a) all growing season months, (b) driest months and (c) the difference between driest and growing season months for varying tree cover fractions and aridity index.
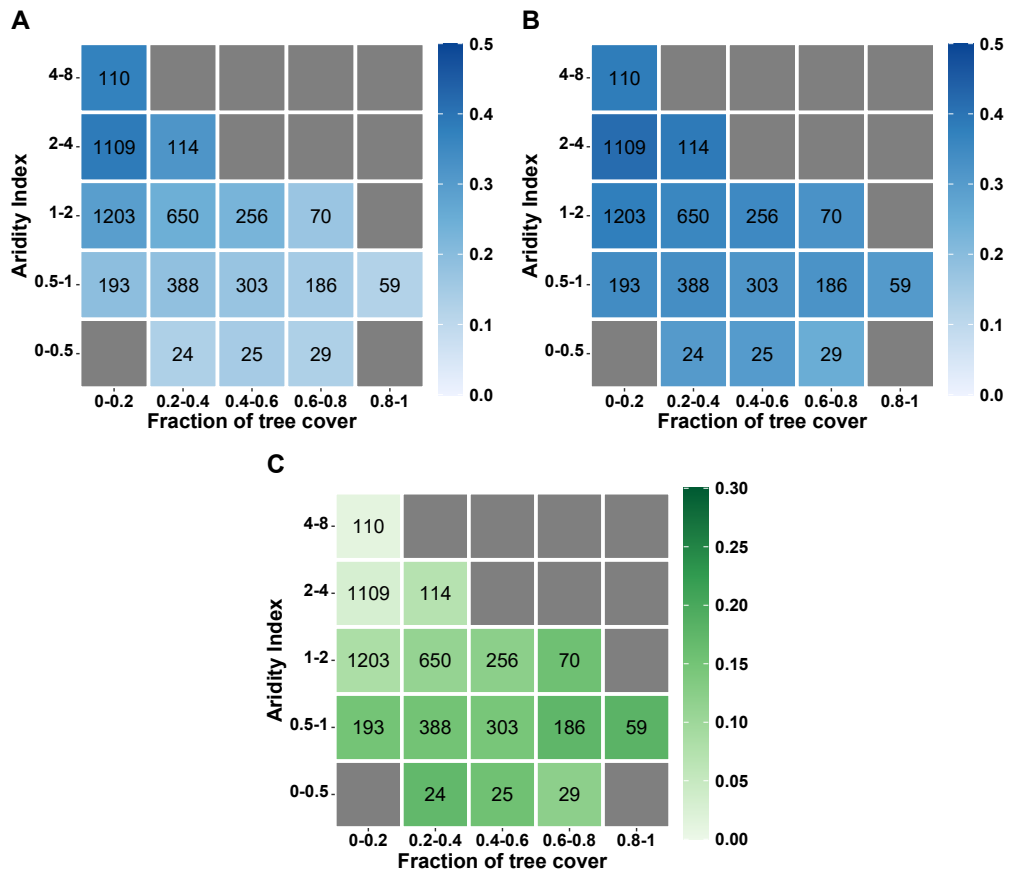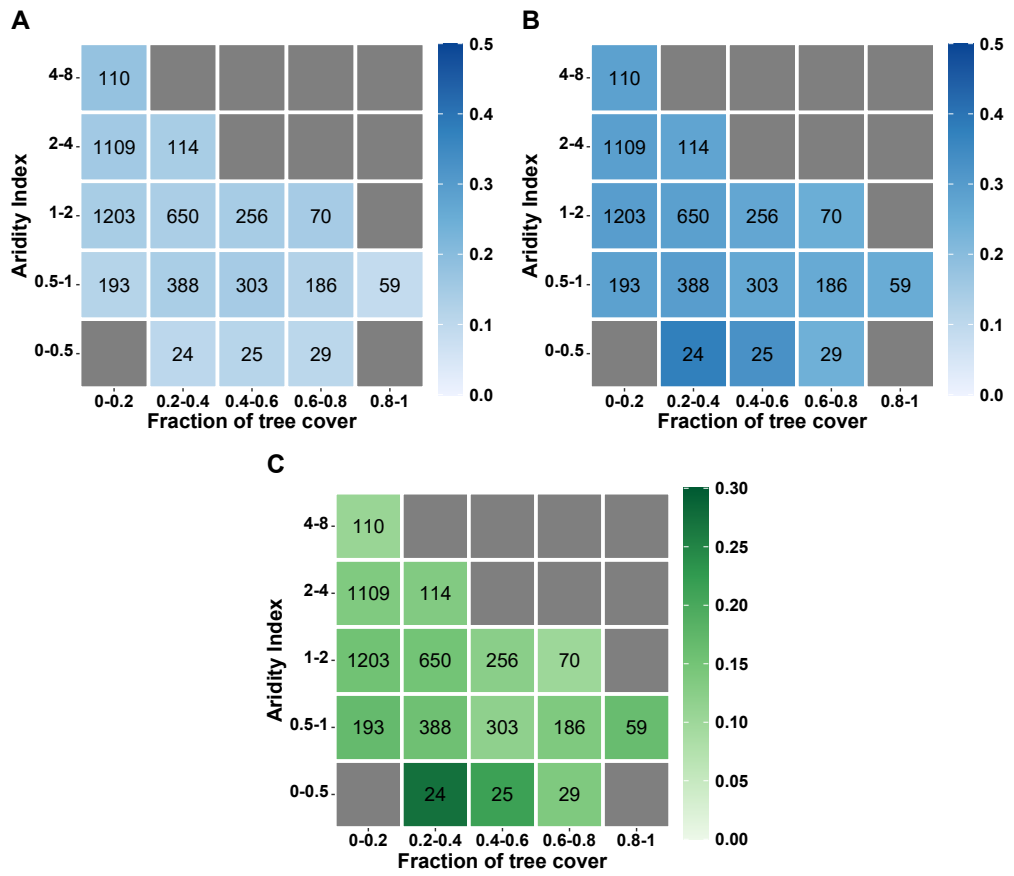
Figure 5.7: Partial correlation of SIF with deep soil moisture in (a) all growing season months, (b) driest months and (c) the difference between driest and growing season months for varying tree cover fractions and aridity index.

Table 5.2 Partial correlation of SIF with (a) surface and (b) deep soil moisture along varying land cover class and aridity index in driest months. For calculating this, each grid cell was assigned to the dominant vegetation type and aridity index. Then, mean correlations are calculated if each vegetation-climate class contains more than 20 grid cells.

(a)

	Aridity Index				
Land Cover Types	0-0.5	0.5-1	1-2	2-4	4-8
Evergreen Needleleaf Forest	-	0.38	0.38	-	-
Evergreen Broadleaf Forest	0.30	0.33	0.36	-	-
Deciduous Broadleaf Forest	-	-	0.26	-	-
Mixed Forest	0.30	0.31	0.27	-	-
Open Shrublands	-	-	0.33	0.45	0.38
Woody Savannas	-	0.37	0.38	0.48	-
Savannas	-	0.37	0.42	0.52	0.54
Grasslands	-	0.37	0.39	0.45	0.48
Croplands	-	0.32	0.38	0.42	0.26

(b)

	Aridity Index				
Land Cover Types	0-0.5	0.5-1	1-2	2-4	4-8
Evergreen Needleleaf Forest	-	0.19	0.43	-	-
Evergreen Broadleaf Forest	0.11	0.15	0.10	-	-
Deciduous Broadleaf Forest	-	-	0.08	-	-
Mixed Forest	0.09	0.12	0.06	-	-
Open Shrublands	-	-	0.19	0.16	0.14
Woody Savannas	-	0.13	0.09	0.15	-
Savannas	-	0.19	0.07	0.09	0.13
Grasslands	-	0.17	0.23	0.16	0.19
Croplands	-	0.15	0.18	0.17	0.24

6 Limitations of the study

We observed an increase in the correlation of SIF with deep moisture in dry months compared to all growing months. However, the partial correlation of SIF with deep soil moisture is still weaker than the partial correlation of SIF with surface soil moisture. This does not align with several site-based isotope tracer studies, which show that the plants rely more on deep soil moisture than surface soil moisture during dry months(Tao et al., 2021; Miguez-Macho and Fan, 2021; Nepstad, 1994).Also, we do not observe significant differences in the correlation between SIF and deep soil moisture between varying vegetation types in both growing season months and dry months. Grasses, in general, have short roots and cannot tap water from the deep layer, but forests and shrubs have deeper roots to take up water in dry months. Hence, the magnitude of correlation increment of r(SIF $\sim$ TWSA), between dry months and growing season months , might vary with differing land cover or tree fraction types. This discrepancy in the our results compared to similar studies might have stemmed from limitations within our study. The disregard of the landscape factor in root water uptake, different signal-to-noise ratios of surface and deep soil moisture products, and the coarser spatial resolution which obfuscates tree cover signals, are major limitations of this study.

The landscape position is a crucial factor in determining vegetation's rooting depth and extent of root water uptake (Fan et al., 2017; Miguez-Macho and Fan, 2021), which is not considered in our analysis. The rooting depth in upland vegetation is shallow because they cannot tap the groundwater due to the large "dry gap" between the surface moisture layer and ground-water. Similarly, the plants on the lowland have shallower roots because of ample moisture availability due to topography-driven drainage. In contrast, plants lying in between upland and lowland, have deeper roots to benefit from seasonal wetting and drying. Hence, the correlation of vegetation with surface and deep soil moisture is likely to differ with landscape positions. Miguez-Macho and Fan (2021) considered the landscape position in finer spatial resolution of 30 arc seconds in their inversion-based modeling of root water uptake globally. Since we study the vegetation-moisture relationship, with only observation-based estimates of vegetation functioning and soil moisture, which are not available at a finer resolution like 30 arc seconds, it is difficult to consider landscape position in our study.

Similarly, potentially different signal-to-noise levels of the surface and deep soil moisture products might affect the comparison of the correlation of SIF with surface and deep soil moisture. The surface soil moisture and deep soil moisture are obtained from different satellites and

have varying processing algorithms, SSM from ESA-CCI and TWSA from GRACE, which lead to different levels of noise associated with each datasets. To overcome this limitation, we additionally incorporate machine learning-based SoMo datasets in the analysis, which has soil moisture in three different layers (0-10 cm, 10-30 cm, 30-50 cm) with a similar noise level between layers. Though the SoMo data facilitate the intercomparison of partial correlation of SIF between three different layers, the correlation results are quite similar between the first and third layers during both growing season months and driest months (See Appendix section A) . This might be because the SoMo datasets are only available up to 50 cm depth, which may not adequately cover deep soil moisture as roots tend to go deeper than 50 cm.

Moreover, the coarse spatial resolution of 0.5-degree further confuscates the vegetation signals. Here, we assign a dominant vegetation type to each grid cell, while such a coarse grid might be composed of different vegetation types. The tree cover fraction also varies largely within such a large grid size, thereby impacting the partial correlation results. This might be one of the important reasons why we do not find differences in the correlation of SIF with deep soil moisture along varying vegetation types and tree cover fractions. This limitation of coarse spatial resolution can be overcome using different datasets for vegetation functioning, which is described in detail in the outlook section (See chapter 8).

In addition, there are several other factors affecting the root water uptake profiles which are not considered in this study but are likely to impact the correlation results. For example, the above-ground biomass and age of vegetation also impact root water uptake, as larger and older trees tend to have deeper roots enabling them to tap deep moisture (Schenk and Jackson, 2002; Tao et al., 2021). The age and above-ground biomass are particularly difficult to consider in global studies due to coarser resolution and the non-availability of adequate observation. Though not so relevant at a monthly time scale, we also do not consider the lagged correlation between SIF and soil moisture.

7 Conclusion

This study illustrates that vegetation photosynthesis is stronger correlated with surface soil moisture compared to deep soil moisture in growing season months. These findings suggest that the vegetation preferentially takes up water from the shallow soil whenever available to meet its transpiration demand. The less energy expenditure in root water uptake, the high concentration of root mass, the less probability of oxygen deficiency, and the ample nutrient availability in the surface layer facilitates the water uptake from the surface soil moisture. Moreover, the partial correlation between vegetation photosynthesis and deep soil moisture follows a similar spatial pattern as that of vegetation photosynthesis with surface soil moisture, indicating that the surface soil moisture observation carries reliable representative information of root zone soil available for vegetation in growing season months.

Moreover, the relationship between vegetation photosynthesis and surface soil moisture differs with varying vegetation and climatic regime. The vegetation photosynthesis strongly correlates with surface soil moisture in regions with low tree cover fractions, such as grasslands, shrublands, and savannas. Besides, for the same vegetation type, the correlation strength between photosynthesis and surface soil moisture increases with an increase in aridity. Hence, grasslands in arid regions, compared to humid regions, are highly correlated with surface soil moisture.

Furthermore, in dry months, vegetation photosynthesis becomes more sensitive to both surface and deep soil moisture compared to growing-season months. The increment in the partial correlation of SIF with surface soil moisture, from growing season months to dry months, is higher in humid regions compared to arid regions. Similarly, we find an increase in correlation between SIF and deep soil moisture during dry months in comparison to growing-season months for all vegetation types. This indicates that the vegetation's dependence on the deep soil moisture increases in dry months, regardless of the vegetation or climatic regimes.

Though there are some limitations in our study (See chapter 6), we could still draw useful scientific conclusions about the role of surface and deep soil moisture in vegetation photosynthesis globally . Besides, some of the limitations like coarser spatial resolution could be overcome in future studies using different datasets and methodologies (See chapter 8)for a better understanding of the role of surface and sub-surface soil moisture in vegetation functioning.

8   Outlook

The limitation of coarser spatial resolution of 0.5 degrees, which confiscates the vegetation signals, could be potentially overcome using observational data in finer spatial resolution. The tree cover fractions and land cover data are available at the spatial resolution of 0.05 degrees, which helps to better disentangle vegetation types, which are presently mixed within grid cells. However, SIF data, from GOME-2, surface, and deep soil moisture observations are not available at such finer spatial resolution. Though efforts have been made to downscale the SIF (Duveiller and Cescatti, 2016), and soil moisture dataset to the finer spatial resolution the uncertainties associated with the downscaling likely impact the correlation results.

As a roundabout, I propose to use NRIvP, which is the product of Near-Infrared Reflectance of Vegetation (NRIv) multiplied by sunlight (P), as an indicator for vegetation functioning. The NRIvP is strongly correlated to far-red SIF across different spatio-temporal scales (Dechant et al., 2022). The NRIv is calculated by multiplying the normalized difference vegetation indices (NDVI) with near infrared reflectance (NIR). The NDVI and NIR can be obtained from the MOD13C1 v006 product (https://lpdaac.usgs.gov/products/mod13c1v006/) in an original 16-day and 0.05° resolution.

Similarly, assuming that the soil moisture anomalies are representative across larger areas, we overcome the limitation of unavailability of the soil moisture datasets at a high resolution of 0.05 degrees. This means, for every grid cell of finer resolution of 0.05 degrees that lies within a coarser grid cell of 0.5 degrees, we assume monthly soil moisture anomalies are uniform and then compute the partial correlation between NRIvP and soil moisture datasets.

Bibliography

R. L. Andrew, H. Guan, and O. Batelaan. Large-scale vegetation responses to terrestrial moisture storage changes. *Hydrol. Earth Syst. Sci.*, 21(9):4469–4478, Sep 2017. ISSN 1607-7938. doi: $10.5194/\text{hess-}21\text{-}4469\text{-}2017$. URL https://hess.copernicus.org/articles/21/4469/2017/.

D. Baldocchi, E. Falge, L. Gu, R. Olson, D. Hollinger, S. Running, P. Anthoni, C. Bernhofer, K. Davis, R. Evans, J. Fuentes, A. Goldstein, G. Katul, B. Law, X. Lee, Y. Malhi, T. Meyers, W. Munger, W. Oechel, K. T. Paw U, K. Pilegaard, H. P. Schmid, R. Valentini, S. Verma, T. Vesala, K. Wilson, and S. Wofsy. Fluxnet: A new tool to study the temporal and spatial variability of ecosystem-scale carbon dioxide, water vapor, and energy flux densities. *Bulletin of the American Meteorological Society*, 82(11):2415–2434, 2001. doi: $10.1175/1520\text{-}0477(2001)082\langle 2415\text{:FANTTS}\rangle 2.3.\text{CO;}2$. URL https://journals.ametsoc.org/view/journals/bams/82/11/1520-0477_2001_082_2415_fantts_2_3_co_2.xml.

S. Bandopadhyay, A. Rastogi, and R. Juszczak. Review of top-of-canopy sun-induced fluorescence (sif) studies from ground, uav, airborne to spaceborne observations, 2020. ISSN 1424-8220. URL https://doi.org/10.3390/s20041144.

K. Berger, M. Machwitz, M. Kycko, S. C. Kefauver, S. Van Wittenberghe, M. Gerhards, J. Verrelst, C. Atzberger, C. van der Tol, A. Damm, U. Rascher, I. Herrmann, V. S. Paz, S. Fahrner, R. Pieruschka, E. Prikaziuk, M. L. Buchaillot, A. Halabuk, M. Celesti, G. Koren, E. T. Gormus, M. Rossini, M. Foerster, B. Siegmann, A. Abdelbaki, G. Tagliabue, T. Hank, R. Darvishzadeh, H. Aasen, M. Garcia, I. Pôças, S. Bandopadhyay, M. Sulis, E. Tomelleri, O. Rozenstein, L. Filchev, G. Stancile, and M. Schlerf. Multi-sensor spectral synergies for crop stress detection and monitoring in the optical domain: A review. *Remote Sensing of Environment*, 280:113198, Oct 2022. ISSN 0034-4257. URL https://www.sciencedirect.com/science/article/pii/S003442572200308X.

G. Bonan. *Ecological Climatology: Concepts and Applications*. Cambridge University Press, Cambridge, 3 edition, 2015. ISBN 9781107619050. doi: $10.1017/\text{CBO}9781107339200$. URL https://www.cambridge.org/core/books/ecological-climatology/D146443B007985BC366B2512345692C0.

W. J. Capehart and T. N. Carlson. Decoupling of surface and near-surface soil water content: A remote sensing perspective. *Water Resources Research*, 33(6):1383–1395, 1997. doi: $10.1029/97\text{WR}00617$. URL https://doi.org/10.1029/97WR00617.

A. Chen, H. Guan, and O. Batelaan. Non-linear interactions between vegetation and terrestrial water storage in australia. *Journal of Hydrology*, 613:128336, Oct 2022. ISSN 0022-1694. URL https://www.sciencedirect.com/science/article/pii/S0022169422009088.

J. L. Chen, C. R. Wilson, B. D. Tapley, L. Longuevergne, Z. L. Yang, and B. R. Scanlon. Recent la plata basin drought conditions observed by satellite gravimetry. *Journal of Geophysical Research: Atmospheres*, 115(D22), Nov 2010. ISSN 0148-0227. doi: 10.1029/2010JD014689. URL https://doi.org/10.1029/2010JD014689.

B. Dechant, Y. Ryu, G. Badgley, P. Köhler, U. Rascher, M. Migliavacca, Y. Zhang, G. Tagliabue, K. Guan, M. Rossini, Y. Goulas, Y. Zeng, C. Frankenberg, and J. A. Berry. Nirvp: A robust structural proxy for sun-induced chlorophyll fluorescence and photosynthesis across scales. *Remote Sensing of Environment*, 268:112763, Jan 2022. ISSN 0034-4257. URL https://www.sciencedirect.com/science/article/pii/S0034425721004831.

J. M. C. Denissen, A. J. Teuling, A. J. Pitman, S. Koirala, M. Migliavacca, W. Li, M. Reichstein, A. J. Winkler, C. Zhan, and R. Orth. Widespread shift from ecosystem energy to water limitation with climate change. *Nature Climate Change*, 12(7):677–684, Jul 2022. doi: 10.1038/s41558-022-01403-8. URL https://doi.org/10.1038/s41558-022-01403-8.

P. A. Dirmeyer, X. Gao, M. Zhao, Z. Guo, T. Oki, and N. Hanasaki. Gswp-2: Multimodel analysis and implications for our perception of the land surface. *Bulletin of the American Meteorological Society*, 87(10):1381–1398, 2006. doi: 10.1175/BAMS-87-10-1381. URL https://journals.ametsoc.org/view/journals/bams/87/10/bams-87-10-1381.xml.

W. Dorigo, W. Wagner, C. Albergel, F. Albrecht, G. Balsamo, L. Brocca, D. Chung, M. Ertl, M. Forkel, A. Gruber, E. Haas, P. D. Hamer, M. Hirschi, J. Ikonen, R. de Jeu, R. Kidd, W. Lahoz, Y. Y. Liu, D. Miralles, T. Mistelbauer, N. Nicolai-Shaw, R. Parinussa, C. Pratola, C. Reimer, R. van der Schalie, S. I. Seneviratne, T. Smolander, and P. Lecomte. Esa cci soil moisture for improved earth system understanding: State-of-the art and future directions. *Remote Sensing of Environment*, 203:185–215, Dec 2017. ISSN 0034-4257. URL https://www.sciencedirect.com/science/article/pii/S0034425717303061.

G. Duveiller and A. Cescatti. Spatially downscaling sun-induced chlorophyll fluorescence leads to an improved temporal correlation with gross primary productivity. *Remote Sensing of Environment*, 182:72–89, Sep 2016. ISSN 0034-4257. URL https://www.sciencedirect.com/science/article/pii/S0034425716301936.

Y. Fan, G. Miguez-Macho, E. G. Jobbágy, R. B. Jackson, and C. Otero-Casal. Hydrologic regulation of plant rooting depth. *Proceedings of the National Academy of Sciences of the United*

States of America, 114(40):10572–10577, Oct 2017. doi: 10.1073/pnas.1712381114. URL https://doi.org/10.1073/pnas.1712381114.

Q. Fang, G. Wang, B. Xue, T. Liu, and A. Kiem. How and to what extent does precipitation on multi-temporal scales and soil moisture at different depths determine carbon flux responses in a water-limited grassland ecosystem? *Science of The Total Environment*, 635:1255–1266, Sep 2018. ISSN 0048-9697. URL https://www.sciencedirect.com/science/article/pii/S0048969718314025.

A. Feldman, D. Gianotti, J. Dong, R. Akbar, W. Crow, K. McColl, J. Nippert, S. J. Tumber-Dávila, N. M. Holbrook, and F. R. e. al. Satellites capture soil moisture dynamics deeper than a few centimeters and are relevant to plant water uptake. *Earth and Space Science Open Archive*, 2022/9/11 2022. doi: 10.1002/essoar.10511280.1DA-2022. URL https://doi.org/10.1002/essoar.10511280.1DA-2022.

A. Geruo, I. Velicogna, J. S. Kimball, J. Du, Y. Kim, A. Colliander, and E. Njoku. Satellite-observed changes in vegetation sensitivities to surface soil moisture and total water storage variations since the 2011 texas drought. *Environmental Research Letters*, 12, 5 2017. ISSN 17489326. doi: 10.1088/1748-9326/aa6965.

L. Guanter, C. Frankenberg, A. Dudhia, P. E. Lewis, J. Gómez-Dans, A. Kuze, H. Suto, and R. G. Grainger. Retrieval and global assessment of terrestrial chlorophyll fluorescence from gosat space measurements. *Remote Sensing of Environment*, 121:236–251, Jun 2012. ISSN 0034-4257. URL https://www.sciencedirect.com/science/article/pii/S0034425712000909.

L. Guanter, Y. Zhang, M. Jung, J. Joiner, M. Voigt, J. A. Berry, C. Frankenberg, A. R. Huete, P. Zarco-Tejada, J.-E. Lee, M. S. Moran, G. Ponce-Campos, C. Beer, G. Camps-Valls, N. Buchmann, D. Gianelle, K. Klumpp, A. Cescatti, J. M. Baker, and T. J. Griffis. Global and time-resolved monitoring of crop photosynthesis with chlorophyll fluorescence. *Proceedings of the National Academy of Sciences*, 111(14):E1327–E1333, Apr 2014. doi: 10.1073/pnas.1320008111. URL https://doi.org/10.1073/pnas.1320008111.

L. Guanter, H. Kaufmann, K. Segl, S. Foerster, C. Rogass, S. Chabrillat, T. Kuester, A. Hollstein, G. Rossner, C. Chlebek, C. Straif, S. Fischer, S. Schrader, T. Storch, U. Heiden, A. Mueller, M. Bachmann, H. Mühle, R. Müller, M. Habermeyer, A. Ohndorf, J. Hill, H. Buddenbaum, P. Hostert, S. Van der Linden, P. J. Leitão, A. Rabe, R. Doerffer, H. Krasemann, H. Xi, W. Mauser, T. Hank, M. Locherer, M. Rast, K. Staenz, and B. Sang. The enmap spaceborne imaging spectroscopy mission for earth observation, 2015. ISSN 2072-4292. URL https://doi.org/10.3390/rs70708830.

M. Heimann and M. Reichstein. Terrestrial ecosystem carbon dynamics and climate feedbacks. *Nature*, 451(7176):289–292, Jan 2008. ISSN 1476-4687. doi: $10.1038/$ $nature06591$. URL https://doi.org/10.1038/nature06591.

H. Hersbach, B. Bell, P. Berrisford, S. Hirahara, A. Horányi, J. Muñoz-Sabater, J. Nicolas, C. Peubey, R. Radu, D. Schepers, A. Simmons, C. Soci, S. Abdalla, X. Abellan, G. Balsamo, P. Bechtold, G. Biavati, J. Bidlot, M. Bonavita, G. De Chiara, P. Dahlgren, D. Dee, M. Diamantakis, R. Dragani, J. Flemming, R. Forbes, M. Fuentes, A. Geer, L. Haimberger, S. Healy, R. J. Hogan, E. Hólm, M. Janisková, S. Keeley, P. Laloyaux, P. Lopez, C. Lupu, G. Radnoti, P. de Rosnay, I. Rozum, F. Vamborg, S. Villaume, and J.-N. Thépaut. The era5 global reanalysis. *Quarterly Journal of the Royal Meteorological Society*, 146(730):1999–2049, Jul 2020. ISSN 0035-9009. doi: $10.1002/qj.3803$. URL https://doi.org/10.1002/qj.3803.

A. J. Hoek van Dijke, M. Herold, K. Mallick, I. Benedict, M. Machwitz, M. Schlerf, A. Pranindita, J. J. E. Theeuwen, J.-F. Bastin, and A. J. Teuling. Shifts in regional water availability due to global tree restoration. *Nature Geoscience*, 15(5):363–368, May 2022. ISSN 1752-0908. doi: $10.1038/s41561-022-00935-0$. URL https://doi.org/10.1038/s41561-022-00935-0.

R. Houborg, M. Rodell, B. Li, R. Reichle, and B. F. Zaitchik. Drought indicators based on model-assimilated gravity recovery and climate experiment (grace) terrestrial water storage observations. *Water Resources Research*, 48(7), Jul 2012. ISSN 0043-1397. doi: $10.1029/$ $2011WR011291$. URL https://doi.org/10.1029/2011WR011291.

V. Humphrey, J. Zscheischler, P. Ciais, L. Gudmundsson, S. Sitch, and S. I. Seneviratne. Sensitivity of atmospheric co2 growth rate to observed changes in terrestrial water storage. *Nature*, 560(7720):628–631, Aug 2018. doi: $10.1038/s41586-018-0424-4$. URL https://doi.org/10.1038/s41586-018-0424-4.

T. F. Keenan and C. A. Williams. The terrestrial carbon sink. *Annual Review of Environment and Resources*, 43(1):219–243, Oct 2018. ISSN 1543-5938. doi: $10.1146/annurev-environ-102017-030204$. URL https://doi.org/10.1146/annurev-environ-102017-030204.

E. N. Koffi, P. J. Rayner, A. J. Norton, C. Frankenberg, and M. Scholze. Investigating the usefulness of satellite-derived fluorescence data in inferring gross primary productivity within the carbon cycle data assimilation system. *Biogeosciences*, 12(13):4067–4084, Jul 2015. ISSN 1726-4189. doi: $10.5194/bg-12-4067-2015$. URL https://bg.copernicus.org/articles/12/4067/2015/.

P. Köhler, L. Guanter, and J. Joiner. A linear method for the retrieval of sun-induced chlorophyll fluorescence from gome-2 and sciamachy data. *Atmos. Meas. Tech.*, 8(6):2589–2608, Jun 2015. ISSN 1867-8548. doi: $10.5194/\text{amt-8-2589-2015}$. URL https://amt.copernicus.org/articles/8/2589/2015/.

P. Köhler, L. Guanter, H. Kobayashi, S. Walther, and W. Yang. Assessing the potential of sun-induced fluorescence and the canopy scattering coefficient to track large-scale vegetation dynamics in amazon forests. *Remote Sensing of Environment*, 204:769–785, Jan 2018. ISSN 0034-4257. URL https://www.sciencedirect.com/science/article/pii/S0034425717304376.

R. D. Koster, Z. Guo, R. Yang, P. A. Dirmeyer, K. Mitchell, and M. J. Puma. On the nature of soil moisture in land surface models. *Journal of Climate*, 22(16):4322–4335, Aug 2009. doi: $10.1175/2009\text{JCLI}2832.1$. URL https://doi.org/10.1175/2009JCLI2832.1.

F. W. Landerer and S. C. Swenson. Accuracy of scaled grace terrestrial water storage estimates. *Water Resources Research*, 48(4), Apr 2012. ISSN 0043-1397. doi: $10.1029/2011\text{WR}011453$. URL https://doi.org/10.1029/2011WR011453.

W. Li, M. Migliavacca, M. Forkel, S. Walther, M. Reichstein, and R. Orth. Revisiting global vegetation controls using multi-layer soil moisture. *Geophysical Research Letters*, 48(11), Jun 2021. doi: $10.1029/2021\text{GL}092856$. URL https://doi.org/10.1029/2021GL092856.

W. Li, M. Migliavacca, M. Forkel, J. M. C. Denissen, M. Reichstein, H. Yang, G. Duveiller, U. Weber, and R. Orth. Widespread increasing vegetation sensitivity to soil moisture. *Nature Communications*, 13(1):3959, Jul 2022. ISSN 2041-1723. doi: $10.1038/\text{s}41467\text{-}022\text{-}31667\text{-}9$. URL https://doi.org/10.1038/s41467-022-31667-9.

F. M.A., A. STRAHLER, and J. HODGES. Islscp ii modis (collection 4) igbp land cover, 2000-2001, 2010. URL http://daac.ornl.gov/cgi-bin/dsviewer.pl?ds_id=968.

Q. . W. J. . Z. S. . T. E. o. R. D. D. f. G. T. Ma, SiyuAU . Wu and C. CCI SM in Yunnan Province. *Remote Sensing*, 9(11), 2017. ISSN 2072-4292. doi: $10.3390/\text{rs}9111124$. URL https://doi.org/10.3390/rs9111124.

X. Ma, A. Huete, J. Cleverly, D. Eamus, F. Chevallier, J. Joiner, B. Poulter, Y. Zhang, L. Guanter, W. Meyer, Z. Xie, and G. Ponce-Campos. Drought rapidly diminishes the large net co2 uptake in 2011 over semi-arid australia. *Scientific Reports*, 6, 2016. doi: $10.1038/\text{srep}37747$. URL https://www.scopus.com/inward/record.uri?eid=2-s2.0-84998771990&doi=10.1038%2fsrep37747&partnerID=40&md5=e2e8cff1fc1ab29d62fb0e815ec82bbf. 37747.

M. Migliavacca, M. Meroni, G. Manca, G. Matteucci, L. Montagnani, G. Grassi, T. Zenone, M. Teobaldelli, I. Goded, R. Colombo, and G. Seufert. Seasonal and interannual patterns of carbon and water fluxes of a poplar plantation under peculiar eco-climatic conditions. *Agricultural and Forest Meteorology*, 149(9):1460–1476, Sep 2009. doi: $10.1016/\mathrm{j.agrformet.}$ $2009.04.003$. URL https://doi.org/10.1016/j.agrformet.2009.04.003.

G. Miguez-Macho and Y. Fan. Spatiotemporal origin of soil water taken up by vegetation. *Nature*, 598(7882):624–628, Oct 2021. doi: $10.1038/\mathrm{s}41586\text{-}021\text{-}03958\text{-}6$. URL https://doi.org/10.1038/s41586-021-03958-6.

G. H. Mohammed, R. Colombo, E. M. Middleton, U. Rascher, C. van der Tol, L. Nedbal, Y. Goulas, O. Pérez-Priego, A. Damm, M. Meroni, J. Joiner, S. Cogliati, W. Verhoef, Z. Malenovský, J.-P. Gastellu-Etchegorry, J. R. Miller, L. Guanter, J. Moreno, I. Moya, J. A. Berry, C. Frankenberg, and P. J. Zarco-Tejada. Remote sensing of solar-induced chlorophyll fluorescence (sif) in vegetation: 50years of progress. *Remote Sensing of Environment*, 231: 111177, Sep 2019. ISSN 0034-4257. URL https://www.sciencedirect.com/science/article/pii/S0034425719301816.

D. C. Nepstad. The role of deep roots in the hydrological and carbon cycles of amazonian forests and pastures. *Nature*, v. 372(no. 6507):pp. 666–669–1994 v.372 no.6507, 1994. doi: $10.1038/372666a0$. URL https://doi.org/10.1038/372666a0.

S. O and R. Orth. Global soil moisture data derived through machine learning trained with in-situ measurements. *Scientific Data*, 8(1), Dec 2021. doi: $10.1038/\mathrm{s}41597\text{-}021\text{-}00964\text{-}1$. URL https://doi.org/10.1038/s41597-021-00964-1.

H. J. Schenk and R. B. Jackson. Rooting depths, lateral root spreads and below-ground/above-ground allometries of plants in water-limited ecosystems. *Journal of Ecology*, 90(3):480–494, Jun 2002. ISSN 0022-0477. doi: $10.1046/\mathrm{j.}1365\text{-}2745.2002.00682.\mathrm{x}$. URL https://doi.org/10.1046/j.1365-2745.2002.00682.x.

S. I. Seneviratne, T. Corti, E. L. Davin, M. Hirschi, E. B. Jaeger, I. Lehner, B. Orlowsky, and A. J. Teuling. Investigating soil moisture-climate interactions in a changing climate: A review, May 2010. URL https://doi.org/10.1016/j.earscirev.2010.02.004.

Z. Tao, E. Neil, and B. Si. Determining deep root water uptake patterns with tree age in the chinese loess area. *Agricultural Water Management*, 249:106810, Apr 2021. ISSN 0378-3774. URL https://www.sciencedirect.com/science/article/pii/S0378377421000755.

A. J. Teuling, M. Hirschi, A. Ohmura, M. Wild, M. Reichstein, P. Ciais, N. Buchmann, C. Ammann, L. Montagnani, A. D. Richardson, G. Wohlfahrt, and S. I. Seneviratne. A regional

perspective on trends in continental evaporation. *Geophysical Research Letters*, 36(2), Jan 2009. ISSN 0094-8276. doi: 10.1029/2008GL036584. URL https://doi.org/10.1029/2008GL036584.

S. Walther, M. Voigt, T. Thum, A. Gonsamo, Y. Zhang, P. Köhler, M. Jung, A. Varlagin, and L. Guanter. Satellite chlorophyll fluorescence measurements reveal large-scale decoupling of photosynthesis and greenness dynamics in boreal evergreen forests. *Global Change Biology*, 22(9):2979–2996, Sep 2016. ISSN 1354-1013. doi: 10.1111/gcb.13200. URL https://doi.org/10.1111/gcb.13200.

S. Walther, L. Guanter, B. Heim, M. Jung, G. Duveiller, A. Wolanin, and T. Sachs. Assessing the dynamics of vegetation productivity in circumpolar regions with different satellite indicators of greenness and photosynthesis. *Biogeosciences*, 15(20):6221–6256, Oct 2018. ISSN 1726-4189. doi: 10.5194/bg-15-6221-2018. URL https://bg.copernicus.org/articles/15/6221/2018/.

J. Wang, X. Xiao, Y. Zhang, Y. Qin, R. B. Doughty, X. Wu, R. Bajgain, and L. Du. Enhanced gross primary production and evapotranspiration in juniper-encroached grasslands. *Global Change Biology*, 24(12):5655–5667, Dec 2018. ISSN 1354-1013. doi: 10.1111/gcb.14441. URL https://doi.org/10.1111/gcb.14441.

X. Wu, X. Xiao, Y. Zhang, W. He, S. Wolf, J. Chen, M. He, C. M. Gough, Y. Qin, Y. Zhou, R. Doughty, and P. D. Blanken. Spatiotemporal consistency of four gross primary production products and solar-induced chlorophyll fluorescence in response to climate extremes across conus in 2012. *Journal of Geophysical Research: Biogeosciences*, 123(10):3140–3161, Oct 2018. ISSN 2169-8953. doi: 10.1029/2018JG004484. URL https://doi.org/10.1029/2018JG004484.

X. Xie, B. He, L. Guo, C. Miao, and Y. Zhang. Detecting hotspots of interactions between vegetation greenness and terrestrial water storage using satellite observations. *Remote Sensing of Environment*, 231:111259, Sep 2019. ISSN 0034-4257. URL https://www.sciencedirect.com/science/article/pii/S0034425719302780.

Y. Yang, D. Long, H. Guan, B. R. Scanlon, C. T. Simmons, L. Jiang, and X. Xu. Grace satellite observed hydrological controls on interannual and seasonal variability in surface greenness over mainland australia. *Journal of Geophysical Research: Biogeosciences*, 119(12):2245–2260, Dec 2014. ISSN 2169-8953. doi: 10.1002/2014JG002670. URL https://doi.org/10.1002/2014JG002670.

S. Z. Yirdaw, K. R. Snelgrove, and C. O. Agboma. Grace satellite observations of terrestrial

moisture changes for drought characterization in the canadian prairie. *Journal of Hydrology*, 356(1):84–92, Jul 2008. ISSN 0022-1694. URL https://www.sciencedirect.com/science/article/pii/S0022169408001716.

P. J. Zarco-Tejada, J. A. J. Berni, L. Suárez, G. Sepulcre-Cantó, F. Morales, and J. R. Miller. Imaging chlorophyll fluorescence with an airborne narrow-band multispectral camera for vegetation stress detection. *Remote Sensing of Environment*, 113(6):1262–1275, Jun 2009. ISSN 0034-4257. URL https://www.sciencedirect.com/science/article/pii/S0034425709000613.

Z. Zeng, L. Peng, and S. Piao. Response of terrestrial evapotranspiration to earth's greening. *Current Opinion in Environmental Sustainability*, 33:9–25, Aug 2018. ISSN 1877-3435. URL https://www.sciencedirect.com/science/article/pii/S1877343517302257.

Y. Zhang, J. Joiner, S. H. Alemohammad, S. Zhou, and P. Gentine. A global spatially contiguous solar-induced fluorescence (csif) dataset using neural networks. *Biogeosciences*, 15(19):5779–5800, Oct 2018. ISSN 1726-4189. doi: $10.5194/\text{bg-}15\text{-}5779\text{-}2018$. URL https://bg.copernicus.org/articles/15/5779/2018/.

Appendices

A   Independent Analysis with SoMo dataset

In the growing season months, the partial correlation of SIF with SoMo soil moisture layers, layer 1 (0-10 cm) (Figure A.1a) and layer 3 (30-50 cm) (Figure A.1b) follow similar global patterns of SIF with surface soil moisture, obtained using ESA CCI soil moisture product. In comparison, the partial correlation of SIF with the SoMo surface layer is slightly higher than the SoMo deep layer globally (Figure A.1c) . Nevertheless, the global patterns of the correlation results of SIF with both the first and third layers look almost similar. This might be because on SoMo layer 3, by model design, contains soil moisture information from SoMo layer 1. This is also plausible physically because, during the overall growing season months, the infiltration connects the upper and lower soil moisture layers hydraulically. Similarly, in dry months, we find the increase in correlation of SIF with SoMo layer 1 (Figure A.2c) and layer 3 (Figure A.3c) compared to overall growing season months. Furtheremore, SIF correlates strongly with layer 1 compared to layer 3 even in dry months.

The analysis involving the SoMo dataset further strengthens the claim that vegetation photosynthesis depends more on shallow soil moisture compared to deep soil moisture in growing-season months. Furthermore, vegetation photosynthesis becomes more sensitive to the overall moisture column (0-50 cm), during dry months compared to growing season months.In contrast to the ESA-CCI SSM and GRACE TWSA datasets which have different noise levels, SoMo layers have similar noise levels. Hence, the conclusion that the vegetation dependence is higher on surface soil moisture compared to deep soil moisture during growing season months holds, regardless of the different noise levels and datasets involved in the analysis.

The major issue with SoMo layers is that they might not well represent soil moisture dynamics as the root tends to go beyond 50 cm, which is different from the deep soil moisture obtained from the GRACE as it represents the overall water column even deeper than 50 cm. This limitation of SoMo might affect the understanding of the relevance of deep soil moisture in vegetation functioning.
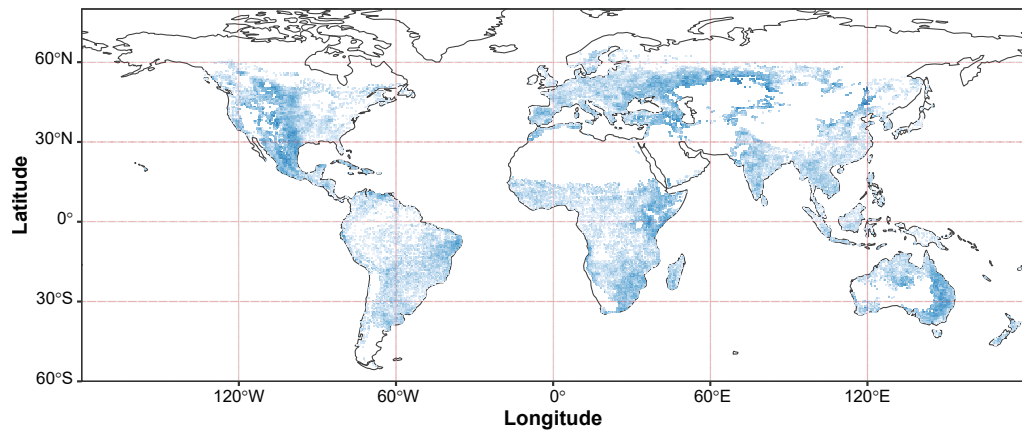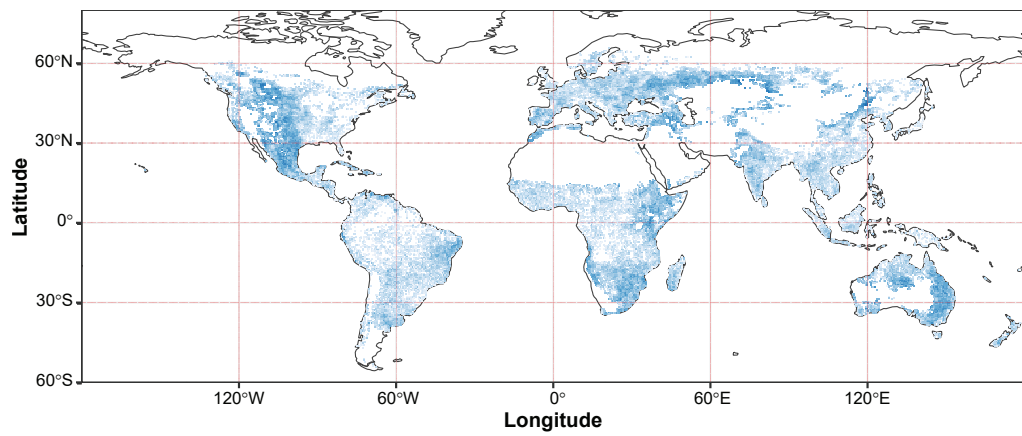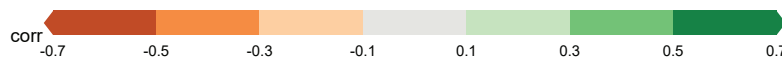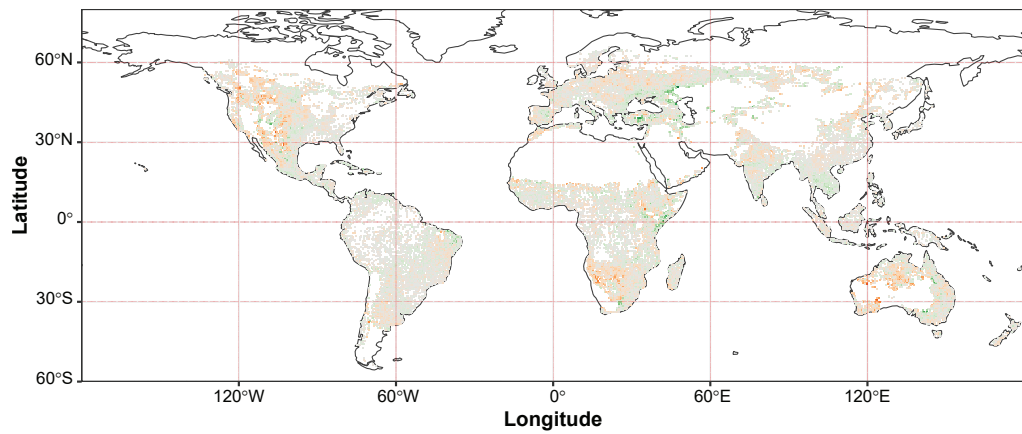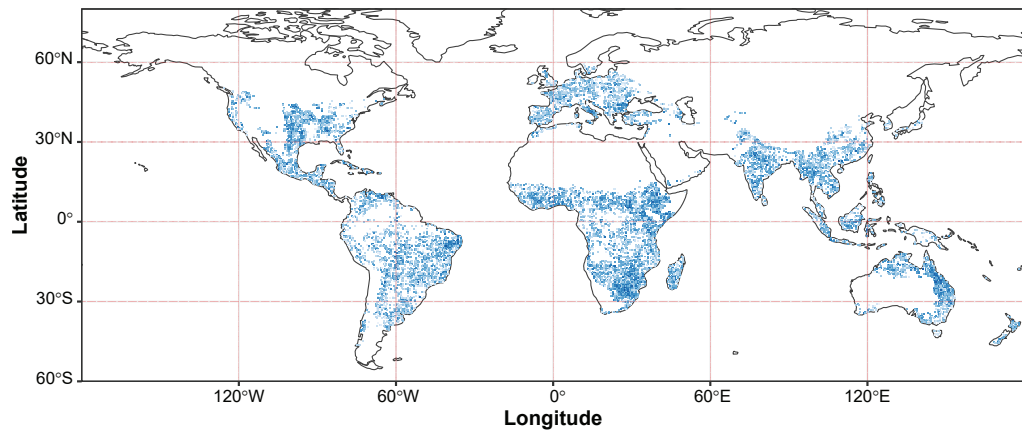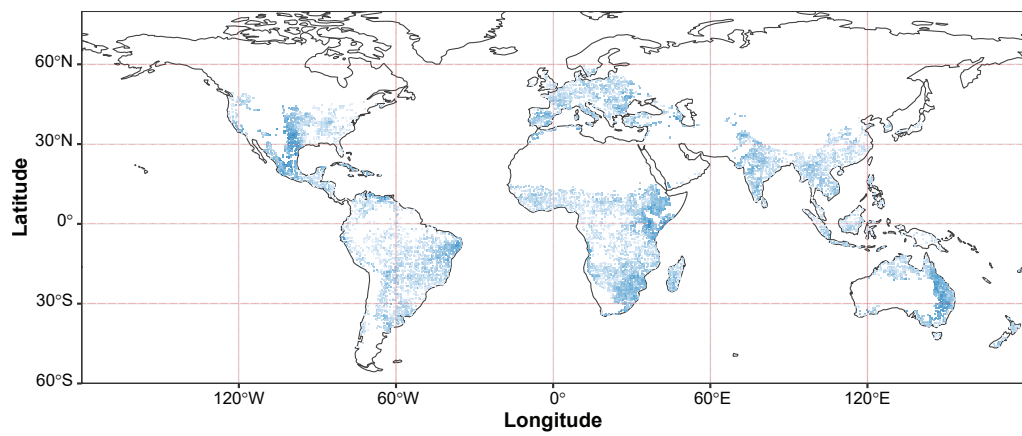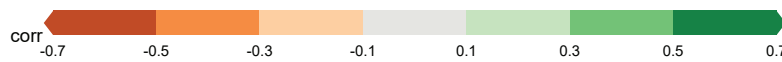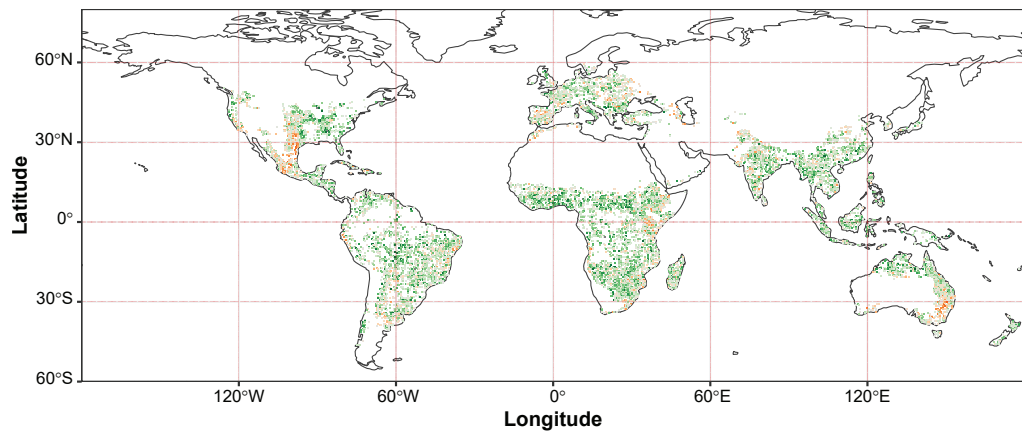
Figure A.1: Partial correlation of SIF with (a) SoMo layer 1 (0-10 cm) and (b) SoMo layer 3 (30-50 cm) and (c) the difference between the SoMo Layer 1 and Layer 3 [a-b].
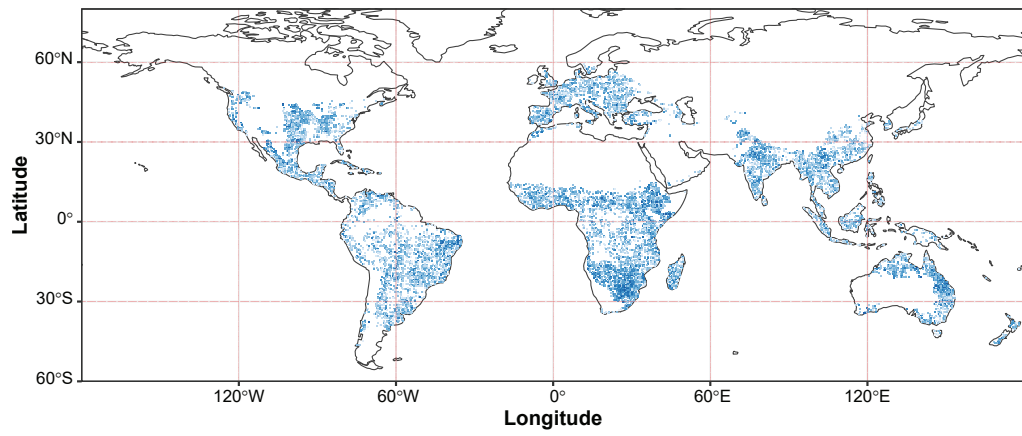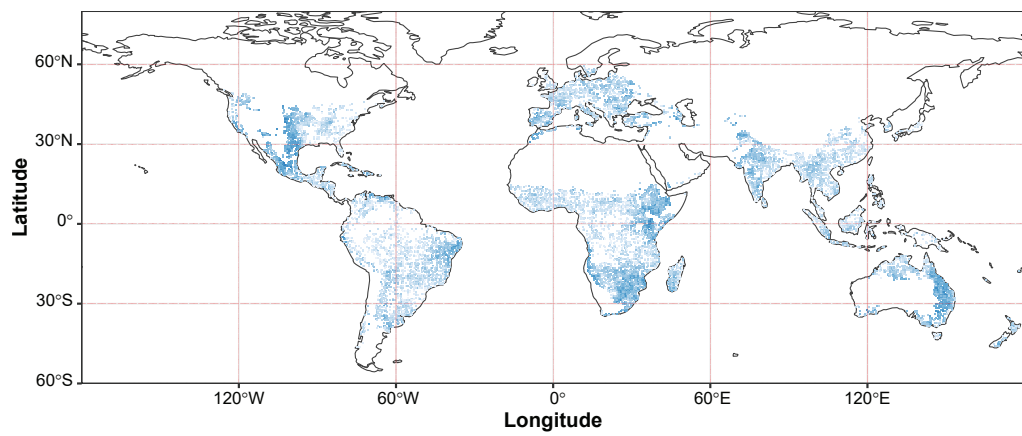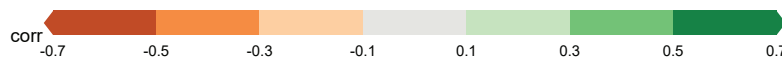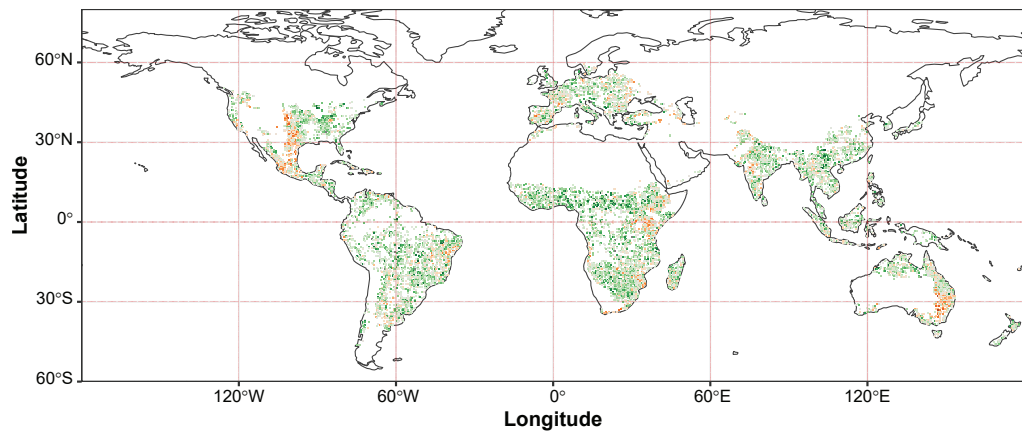
Figure A.2: Partial correlation of SIF with SoMo layer 1 (0-10 cm) in (a) driest and (b) all growing season months and (c) difference between driest and growing season months [a-b].

Figure A.3: Partial correlation of SIF with SoMo layer 3 (30-50 cm) in (a) driest and (b) all growing season months and (c) difference between driest and growing season months [a-b].

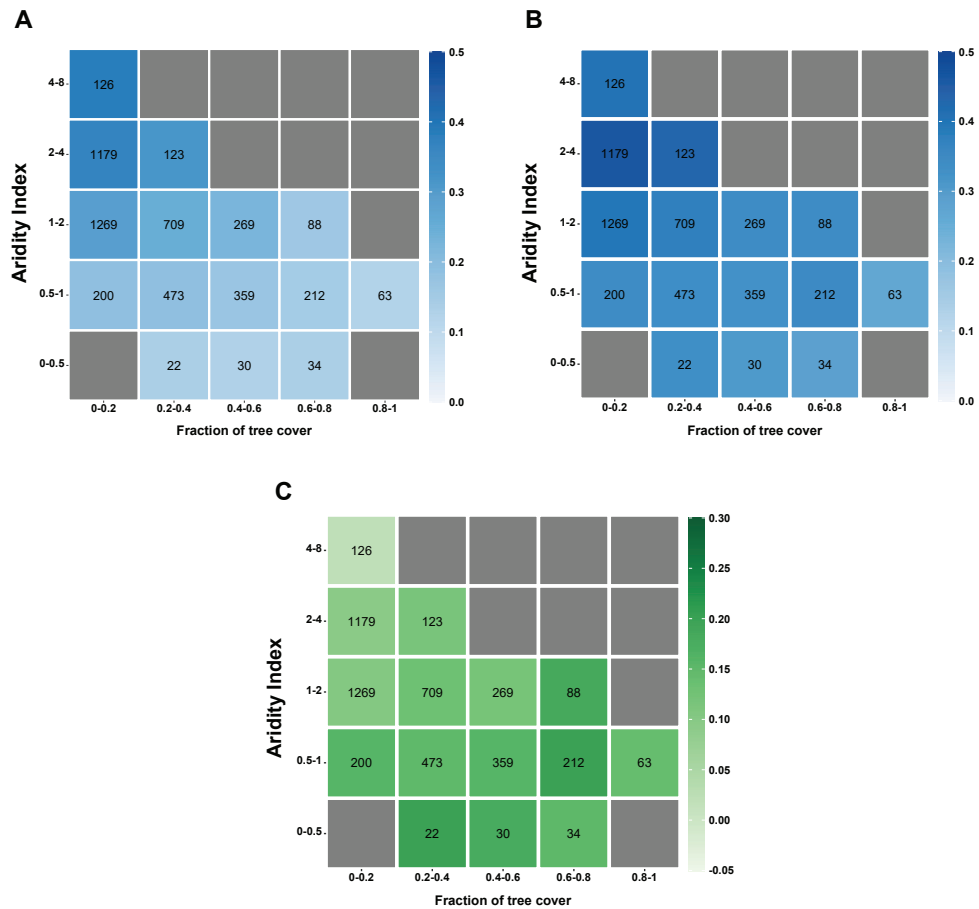# B Partial correlation for the driest months defined by lowest absolute value of surface soil moisture

Figure B.4: Partial correlation of SIF with surface soil moisture in (a) all growing season months, (b) driest months and (c) the difference between driest and growing season months for varying tree cover fractions and aridity index. The driest months is defined by the 15 lowest absolute values of SSM, in contrast to the (Figure 5.6), where driest months are defined by the 15 lowest absolute values of TWSA. This helps to conclude that the method of selection of dry months do not impact our overall results.
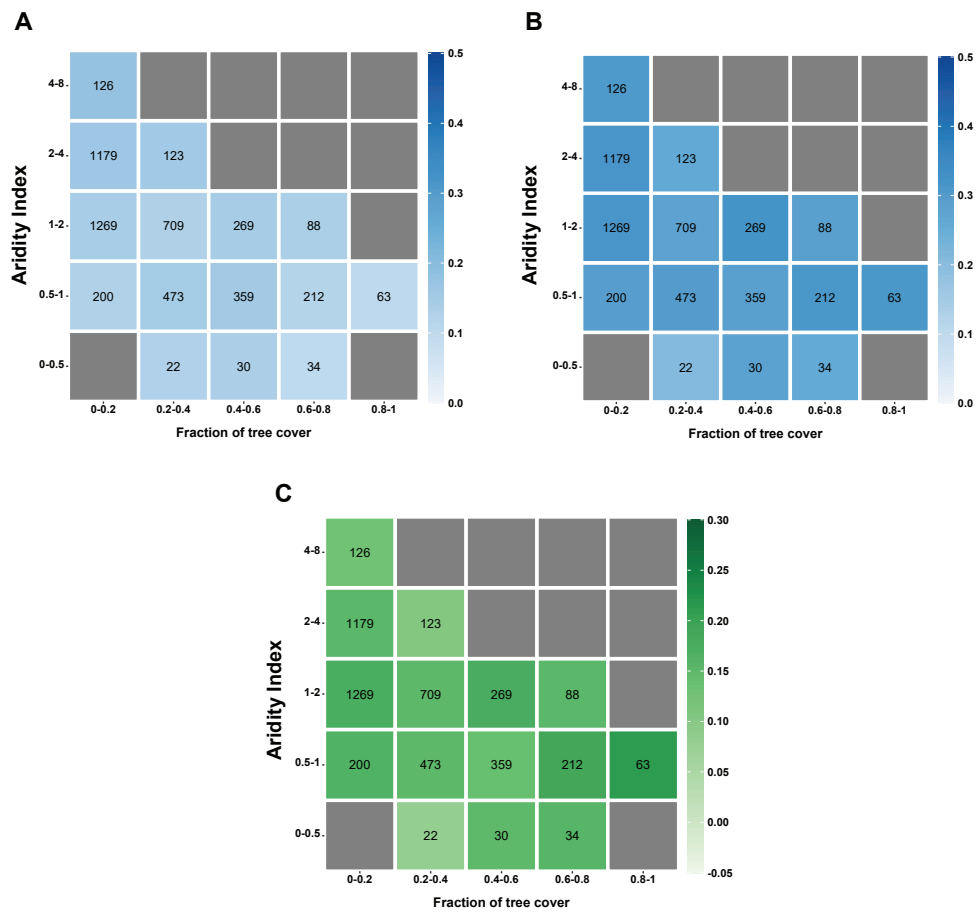
Figure B.5: Partial correlation of SIF with deep soil moisture in (a) all growing season months, (b) driest months and (c) the difference between driest and growing season months for varying tree cover fractions and aridity index. The driest months is defined by the 15 lowest absolute values of SSM, in contrast to the (Figure 5.7), where driest months are defined by the 15 lowest absolute values of TWSA. This helps to conclude that the method of selection of dry months do not impact our overall results.

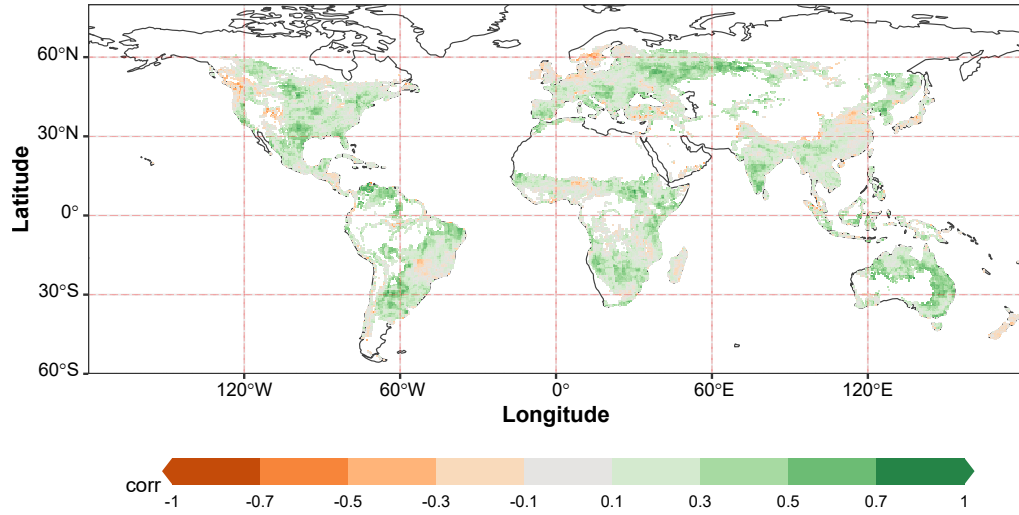# C Correlation between SSM and TWSA in growing season months

Figure C.6: Correlation of SSM with TWSA in the growing season months. This shows that the SSM and TWSA are highly correlated in most regions globally in the growing season months.